TU Delft

Delft University of Technology

Beyond Double-Double theory: n-Directional stacking sequence optimisation in composite laminates

José Humberto S. Almeida, Jr; Balonek, Emilia; Castro, Saullo G.P.

DOI
10.1016/j.compstruct.2025.119586

Publication date
2025

Document Version
Final published version

Published in
Composite Structures

Citation (APA)
José Humberto S. Almeida, J., Balonek, E., & Castro, S. G. P. (2025). Beyond Double-Double theory: n-Directional stacking sequence optimisation in composite laminates. *Composite Structures*, *373*, Article 119586. https://doi.org/10.1016/j.compstruct.2025.119586

Important note
To cite this publication, please use the final published version (if applicable).
Please check the document version above.

Copyright
Other than for strictly personal use, it is not permitted to download, forward or distribute the text or part of it, without the consent of the author(s) and/or copyright holder(s), unless the work is under an open content license such as Creative Commons.

Takedown policy
Please contact us and provide details if you believe this document breaches copyrights.
We will remove access to the work immediately and investigate your claim.

This work is downloaded from Delft University of Technology.
For technical reasons the number of authors shown on this cover page is limited to a maximum of 10.

Composite Structures 373 (2025) 119586

Contents lists available at ScienceDirect

Composite Structures

journal homepage: www.elsevier.com/locate/compstruct

Beyond Double-Double theory: *n-Directional* stacking sequence optimisation in composite laminates

José Humberto S. Almeida Jr. [a,*], Emilia Balonek [a], Saullo G.P. Castro [b,*]

[a] Department of Mechanical Engineering, LUT University, Lappeenranta, Finland
[b] Department of Aerospace Structures & Materials, Delft University of Technology, Kluyverweg 1, Delft, The Netherlands

ARTICLE INFO

Keywords:
Double-Double theory
Novel *n-Double* theory
Optimisation
Buckling
Failure

ABSTRACT

This paper presents a novel stacking sequence design framework for composite laminates, extending the recently established Double-Double (*DD*) laminate theory developed by Stephen Tsai. By introducing and evaluating *n-Double (n-D)* layouts, ranging from single-angle (*D*) sequences to multi-directional designs such as *DD*, *DDD*, and *DDDD*; this study expands the design space for laminated composite structures, enabling improved trade-offs between buckling resistance and failure strength. A genetic algorithm (GA) is used to optimise the stacking sequences of 48- and 64-layer graphite/epoxy laminates under biaxial and uniaxial compressive loading across a range of geometric aspect ratios. Results show that while GA-based free-angle designs yield the highest buckling loads, structured *DDDD* configurations achieve similar or superior failure performance and maintain a high level of robustness across geometric variations. The *DDDD* designs also approximate GA-level buckling performance, with significantly improved regularity and manufacturability. These findings highlight the benefit of generalising Tsai's *DD* theory towards *n-D* layouts, providing a systematic, practical, and high-performing approach to laminate optimisation.

1. Introduction

In recent years, several works have emerged around the use of general stacking sequences that are not restricted by traditional assumptions such as symmetry, balance, or the 10% rule (i.e., each fibre orientation used in the laminate must account for at least 10% of the total number of plies). Among these, the polar method and the multi-scale multi-level optimisation strategies have proven particularly powerful [1,2]. This formalism allows the identification of optimal stacking sequences without enforcing unnecessary constraints, thereby enabling superior mechanical performance [3–6].

While these advanced methods explore the full potential of anisotropic tailoring, traditional quasi-isotropic (quad) laminates, characterised by balanced and symmetric stacking and often referred to as "black metal" designs, remain prevalent in aeronautical and aerospace applications. These configurations have historically played a central role in composite structural design, but their inherent limitations have constrained the broader adoption of composites in high-performance applications. One challenge lies in the combinatorial complexity of stacking sequence permutations, which grows rapidly with ply count and complicates optimal design identification [7]. Additionally, quad laminates can exhibit shear coupling in their flexural stiffness components, adding difficulty in structural analysis and optimisation [8]. These limitations motivate the exploration of structured yet more flexible stacking approaches, such as the proposed *n-D* framework.

Another major limitation of quad laminates is the challenge of achieving homogenisation while maintaining practical thickness constraints. Homogenisation in composite laminates often requires a substantial number of plies, sometimes reaching up to 120, which results in increased structural thickness. This characteristic is particularly problematic in applications where minimal gauge thickness is essential, such as lightweight aerospace structures. Furthermore, the requirement for mid-plane symmetry further constrains laminate design and results in manufacturing inefficiencies. The difficulty in producing thin, lightweight composite laminates with uniform mechanical properties has limited the potential advantages of composites over conventional materials [9].

Additionally, limitations in tapering and ply dropping further restrict the effectiveness of quad laminates in practical applications. Achieving weight reduction in composite structures often requires the selective removal of plies, but this process is problematic in quad laminates. When plies are dropped to create a taper, the laminate properties are altered, leading to potential reductions in structural performance. Furthermore, ply dropping in quad laminates can introduce manufacturing defects, such as resin-rich areas or voids, which

* Corresponding authors.
E-mail addresses: humberto.almeida@lut.fi (J.H.S. Almeida Jr.), S.G.P.Castro@tudelft.nl (S.G.P. Castro).

https://doi.org/10.1016/j.compstruct.2025.119586
Received 3 April 2025; Received in revised form 15 July 2025; Accepted 19 August 2025
Available online 25 August 2025
0263-8223/© 2025 The Authors. Published by Elsevier Ltd. This is an open access article under the CC BY license (http://creativecommons.org/licenses/by/4.0/).

compromise mechanical integrity. These challenges make it difficult to efficiently design composite structures that balance both strength and weight optimisation [10]. Additionally, in contrast to Quasi-Trivial (QT) stacks [3], which provide exact solutions to membrane/bending uncoupling and homogeneity conditions regardless of ply angle values, *DD* configurations only approximate these properties and typically require a higher number of plies to do so. Moreover, *DD* stacks are generally orthotropic in membrane behaviour but remain anisotropic in bending, potentially limiting their stiffness tailoring capability. Recent advances [2] have further shown that general ply-drop propagation rules, based on the concept of search propagation direction, can be formulated independently of the stacking sequence type. These developments position *DD* stacks as a practical yet constrained subset within the broader laminate design landscape.

To address these limitations, Double–Double laminates have been proposed by Stephen Tsai [11] as an alternative approach in the design and manufacturing of composites, offering several key advantages over traditional quad laminates. The DD laminate concept simplifies design by utilising a consistent four-ply building block, significantly reducing the complexity associated with stacking sequences. This simplification enables more efficient laminate design while maintaining desirable mechanical properties. Additionally, *DD* laminates can achieve homogenisation with fewer plies allowing for thinner, lightweight structures that meet performance requirements. Unlike quad laminates, *DD* laminates enable more effective tapering without altering laminate properties, facilitating weight reduction without introducing structural deficiencies. By overcoming the key drawbacks of quad laminates, *DD* laminates present a promising approach for optimising composite structures, particularly in aerospace and high-performance engineering applications.

The *DD* laminate stacking sequence replaces traditional quasi-isotropic quad laminates (e.g., $[0/45/-45/90]_S$) with a new form: $(\pm\theta, \pm\phi)$ repeating angles. This approach aims to increase efficiency by reducing ply discontinuities, stress concentrations, and ply drop-offs. The main benefits of *DD* layouts are:

- Simplified stacking sequence: The DD layup uses two pairs of angle-plies, which simplifies the design and manufacturing processes. This configuration reduces the number of plies required, thereby decreasing the overall weight of the composite structure [9];
- Improved manufacturability: The *DD* method facilitates through-the-thickness homogenisation using thinner sub-laminates. This allows for profile optimisation through thickness tapering, making the manufacturing process more efficient and less prone to errors [11];
- Damage resistance and tolerance: Studies comparing DD laminates with traditional quad laminates have shown that *DD* laminates exhibit comparable damage resistance and tolerance. This is evident from the similar magnitudes of delaminated areas observed in both types of laminates after impact and compression after impact (CAI) tests [12];
- Weight reduction: The DD design has been shown to significantly reduce composite structure weight. For instance, an optimised *DD* design for a composite stiffened panel in the aviation field achieved a mass reduction of up to 26.48%, contributing to improved fuel efficiency and operational performance [13]; and
- Enhanced structural performance: The *DD* laminates offer improved structural performance by mitigating the warpage of non-symmetric laminates. This is achieved through layup homogenisation, which ensures the structural integrity of the composite material [11].

To better understand this new type of stacking sequence and its progress so far, a complete, yet non-extensive, state-of-the-art review is presented next.

1.1. The state-of-the-art

Table 1 summarises key journal publications addressing *DD* laminates, focusing on their optimisation methodologies, applications, and main findings. The table highlights how *DD* laminates have been predominantly developed through stiffness homogenisation approaches, with some recent efforts exploring their buckling and damage tolerance behaviour under specific loading cases.

1.2. Motivation and gap

As outlined in the state-of-the-art review (Section 1.1), the Double-Double (*DD*) laminate design theory has demonstrated clear advantages over traditional quasi-isotropic (Quad) laminates, including enhanced structural efficiency, reduced weight, and improved manufacturability through homogenised stiffness design. However, the *DD* concept remains constrained by its four-ply repeated substructure, potentially limiting its applicability in fully exploiting the design space of multi-angle fibre-reinforced laminates for advanced structural applications.

To unlock further gains in buckling resistance, failure strength, and directional stiffness tailoring, this study explores the generalisation of the *DD* concept towards *n-Double (n-D)* laminates. These configurations extend the design space from single-angle *D* to *DDDD* layouts with up to four unique ply angles, enabling multi-directional tailoring. Such an approach is especially promising for critical loading cases, including uniaxial and biaxial compression, commonly encountered in aerospace, automotive, and high-performance engineering structures.

Despite the potential benefits, several research gaps remain unaddressed:

- Existing *DD* laminates primarily focus on stiffness matching with reference designs and may not be optimal for performance under uniaxial or biaxial loading conditions;
- The exploration of stacking sequences beyond four angles (*e.g.*, *DDD* and *DDDD*) has not yet been systematically investigated for structural performance enhancement;
- Current design methods rely on trial and error-based stiffness matching, whereas the use of genetic algorithms (GA) offers a more robust and global approach to stacking sequence optimisation; and
- Additional design constraints, such as manufacturability, layup symmetry, and gradual thickness transitions, need to be integrated into optimisation frameworks to ensure practical feasibility.

Addressing these gaps through a systematic optimisation and evaluation framework will pave the way for novel, high-performance laminate architectures with tailored responses and increased robustness across a broad range of operating conditions.

1.3. Aim of this study

This work aims to develop a comprehensive optimisation framework for *n-D* laminates by generalising Tsai's Double-Double (*DD*) theory to include both lower- and higher-order stacking sequences, from *D* to novel *DDDD* layouts. Two complementary strategies are employed: stiffness matching and heuristic optimisation via a GA. The objective is to maximise structural performance by improving buckling and failure load factors of laminated plates subjected to uniaxial and biaxial compressive loads. Additionally, five aspect ratios (a/b, the ratio of longitudinal to lateral dimensions) are investigated to capture geometric effects.

The proposed methodology consists of three key steps:

1. Stiffness matching: Extending the homogenisation-based design approach to generate *n-D* layups with equivalent in-plane stiffness to reference laminates under biaxial and uniaxial compressive loading;

Table 1
The current state-of-the-art on *DD* laminates.

Ref.	Loading	Approach	Main results
[9]	Internal pressure, bending and buckling	Trial-and-error	DD can be up to 50% lighter than Quad laminates
[14]	Uncertain loads	GA	8.5% mass savings compared to Quad laminates while balancing laminates about principal loading axes reduces mass by 20%
[15]	Bending, torsion, and thermal	FEA & optimisation (GA)	DD laminates warp less than Quad/D; both D and DD show superior thermal behaviour enabling up to 70% mass reduction
[16]	Uniaxial compression and shear	FEA & optimisation & analytical	The DD method speeds homogenisation, cuts costs, and reduces weight beyond Quad laminates
[17]	Uniaxial compression	Nonlinear FEA and GA optimisation	The manufacturing process significantly impacts the axial load-carrying capacity and transition load of unsymmetric laminates
[18]	Multiple loads	Topology optimisation	Structures designed with several failure criteria - Tsai–Wu criterion reached the lowest failure index
[19]	Uniaxial compression	Analytical, experimental	Layup homogenisation reduces warpage by 97.5% with eight repetitions of asymmetric cross-ply sub-laminates
[20]	Open-hole tension and compression & Low-Velocity Impact (LVI)	Machine learning (ML), analytical & FEA	Gaussian Processes perform well with small datasets and Artificial Neural Networks excel with larger datasets. The models accurately capture the statistical distribution of notched strength
[21]	Compression loads	Experimental and optimisation (GA)	DD designs enhance buckling, remove bending–twisting coupling, and optimise stiffness in compression members
[22]	Multiple loads	Machine learning	Ridge regression is the most effective model, achieving 99% accuracy and being 1000 times faster than FE simulations
[23]	LVI & compression	Experiments	DD laminates show superior impact resistance and energy absorption, with mechanical properties close to Quad
[24]	Bending and torsion	FE and analytical models	The lightest DD laminate is found for a given buckling load, avoiding extensive evaluations of Quad laminates
[25]	Multiple loads	Topology optimisation	Optimised configurations obtained by DD and Quad are similar
[26]	Tension and compression	Experimental, FEA & optimisation	DD design demonstrates superior energy absorption compared to Quad configurations
[27]	Various loads	Numerical and experimental	DD laminates exceed Quad in damage onset and stress distribution, with up to 25.8% higher performance
[24]	Bending, tensile, and shear	Analytical	Validation confirms that ξ_{A1} and ξ_{A2} equal ξ_{D1} and ξ_{D2}, while ξ_{A3} and ξ_{A4} are zero
[28]	Compression	Compliance Beam Method	DD layup increases maximum load by 13% and shear fracture energy by 38%. Also, DD laminates delay crack propagation
[29]	Varying damage initiation loads	Analytical	The first DD optimum solution for the 'horse-shoe' use case achieves a 7.8% weight reduction
[30]	Various loading conditions	Deep transfer ML	Transfer learning enhances the generalisation of ML models for both known and new design parameters
[31]	Mode-I fracture toughness	Modified beam theory (MBT) method	Enhanced crack mitigation with DD layups
[32]	Multiple loading conditions	Optimisation, FE simulations	The redesign process achieved up to 29% mass reductions while maintaining mechanical performance
[33]	Multiple loading conditions	"DD Automated Design Tool", GA	DD laminates enabled a 64.6% weight reduction compared to Quad laminates
[13]	LVI	Experimental and numerical	The DD design cut mass by up to 71% in frames and 13% in the fuselage while preserving crashworthiness
[12]	Compression	Analytical	The DD laminate exhibited higher uniaxial compressive strength and stiffness with increases of 24% and 11%, respectively
[34]	Bending and torsion	Semi-analytical and experimental	Steady-state *R*-curves with DD laminates
[35]	Compression	Analytical	The DD formulation simplifies design, cuts computation, reduces weight, and boosts early design maturity
[36]	LVI & CAI	Optimisation and FEA	The angle optimisation design of DD laminates is crucial for performance improvement and weight reduction
[37]	Compression	FEA	The $\left[67.5°/-22.5°/22.5°/-67.5°\right]_{8T}$ laminate shared the $[A^*]$ matrix, showing CAI behaviour similar to Quad
[38]	Fatigue	Experimental	DD laminates showed smaller damage in static/dynamic tests, with better homogenisation and weight reduction
[39]	Shear	Analytical, optimisation, FEA	Simplified laminate design and manufacturing processes. Layup homogenisation effectively mitigated warpage in asymmetric layups
[40]	Uniaxial compression and shear	FEA	DD laminates offer improved performance over Quad laminates in specific loading scenarios
[41]	Buckling	FEA, optimisation	Spacing constraints yield smoother thickness transitions with slight performance loss

2. Heuristic optimisation: Implementing a GA to explore the optimum stacking sequences that maximise buckling resistance and delay failure onset for each a/b case and stacking layout constraint; and
3. Structural performance evaluation: Comparing the optimised *n-D* laminates to conventional Quad designs through numerical simulations to assess improvements in load-bearing capacity, robustness, and design flexibility.

The paper is organised as follows. Section 1 provides the introduction, a comprehensive state-of-the-art review (Section 1.1), the motivation and research gap (Section 1.2), and the aim of the study in Section 1.3. Section 2 outlines the proposed generalised formulation in Section 2.1, followed by the implementation of the linear buckling analysis in Section 2.2 and the optimisation problem and characteristics (Section 2.3). Section 3 presents the numerical results, including the Direct Stiffness Matching approach (Section 3.1), convergence analysis of the optimisation process (Section 3.2), buckling optimisation results (Section 3.3), and an analysis of the optimum stacking sequences (Section 3.4). Section 4 discusses the key findings, with emphasis on stiffness matching and design generalisation (Section 4.1), the buckling and failure behaviour under uniaxial and biaxial compression for the 48-ply laminate (Section 4.2), the limitations observed in the 64-ply laminate (Section 4.3), the broader implications for structural laminate design (Section 4.4), the polar plots in Section 4.5, and the overall limitations of this study are listed in Section 4.6. Finally, Section 5 summarises the main conclusions of the study.

2. Methodology

2.1. Generalised n-Double laminates

Double–double (DD) laminates, characterised by a two-angle stacking sequence of the form $[\pm\phi, ; \pm\psi]$, can be extended to an *n-D* laminate defined by $[\pm\phi_1, ; \pm\phi_2, \ldots, \pm\phi_n]$. In this generalised family, each ϕ_k (with $k = 1, \ldots, n$) is a distinct ply orientation (typically $0° \leq \phi_k \leq 90°$ due to symmetry), and each appears as a balanced $\pm\phi_k$ pair. By increasing n, a broader design space of stiffness properties can be achieved, approaching quasi-isotropic behaviour as n grows. Higher values of n (e.g., $n = 3$ or 4) introduce additional ply angles for fine-tuning stiffness anisotropy but at the cost of more complex stacking sequences.

Assuming a symmetric and balanced *n-D* laminate (hence neglecting elastic coupling, with $[B] = \mathbf{0}$), the in-plane extensional stiffness matrix $[A]$ can be expressed in terms of the lamina invariants and the ply angles ϕ_k. We adopt the trace-normalised invariant framework of Tsai and Melo [8,42], which defines an orientation-invariant scalar "trace" of the reduced stiffness: $Tr = Q_{11} + Q_{22} + 2Q_{66}$; for a single ply stiffness matrix $[Q]$ in plane stress. Using this invariant Tr as a normalising factor, one defines a dimensionless stiffness matrix $[Q^*] = [Q]/Tr$, which is invariant to overall material stiffness scale. The transformed stiffness of a ply at orientation θ can then be written as a linear combination of trace-normalised invariants U_i^* multiplied by simple trigonometric functions of θ. In particular, the in-plane stiffness components take the form [42]:

$$\bar{Q}^*_{11}(\theta) = U_1^* + U_2^* \cos 2\theta + U_3^* \cos 4\theta \tag{1}$$

$$\bar{Q}^*_{22}(\theta) = U_1^* - U_2^* \cos 2\theta + U_3^* \cos 4\theta \tag{2}$$

$$\bar{Q}^*_{12}(\theta) = U_4^* - U_5^* \cos 4\theta \tag{3}$$

and similarly for $\bar{Q}^*_{66}(\theta)$. Here, the $\bar{Q}^*_{ij}$ are dimensionless rotated stiffness coefficients in the laminate coordinate system, and U_i^* are invariant material parameters that are dependent on the Q_{ij} values of the plies, but not on θ. For example, one of these invariants is given by $U_1 = \frac{3}{8}(Q_{11} + Q_{22}) + \frac{1}{4}Q_{12} + \frac{1}{2}Q_{66}$, which when normalised by the trace yields U_1^*. The set $\{U_1^*, U_2^*, U_3^*, U_4^*, U_5^*\}$, often named Tsai's invariants, provides an invariant description of the in-plane ply stiffness properties. Using the relations in Eqs. (1) to (3), the extensional stiffness A_{ij} of an *n*-double laminate can be obtained by summing the contributions of all plies. Thanks to the balanced $\pm\phi_k$ pairs, all terms involving $\sin 2\theta$ or $\sin 4\theta$ cancel out, and only even cosine terms remain. If each orientation ϕ_k is represented with an equal fraction of plies (a common assumption in a homogenised laminate), the in-plane A-matrix components can be written in closed form. For instance, defining the average cosine factors

$$\langle \cos 2\phi \rangle = \frac{1}{n}\sum_{k=1}^{n} \cos 2\phi_k \,, \qquad \langle \cos 4\phi \rangle = \frac{1}{n}\sum_{k=1}^{n} \cos 4\phi_k \,,$$

the normalised in-plane stiffness terms become:

$$\frac{A_{11}}{h\,\mathrm{Tr}} = U_1^* + U_2^* \langle \cos 2\phi \rangle + U_3^* \langle \cos 4\phi \rangle \,, \tag{4}$$

where h is the laminate thickness. Analogous expressions hold for A_{22}, A_{12}, A_{66}, and so forth. Eq. (4) is obtained by inserting the $\pm\phi_k$ ply contributions from Eqs. (1)–(3) into the definition $A_{ij} = \sum_{\text{plies}} \bar{Q}_{ij} Tr, \Delta z$ (summing over ply thickness). The anti-symmetry of the laminate ensures $A_{16} = A_{26} = 0$, and the in-plane stiffness is fully described by Eq. (4) (along with all A_{ij}, which can be written in a similar invariant form). Notably, the combination U_1^* corresponds to the trace-normalised isotropic part of the stiffness (it equals $\frac{1}{8}(Q_{11} + Q_{22} + 2Q_{12} + 4Q_{66})/Tr$, i.e. the orientation-averaged stiffness), while U_2^* and U_3^* govern the orthotropic deviations (associated with $\cos 2\theta$ and $\cos 4\theta$ dependence). In a fully quasi-isotropic limit (infinitely many angles or a continuous distribution), $\langle \cos 2\phi \rangle \to 0$ and $\langle \cos 4\phi \rangle \to 0$, so that $A_{11} = A_{22} = hTrU_1^*$ and $A_{12} = hTrU_4^*$; recovering an isotropic in-plane stiffness characterised essentially by a single modulus Tr, U_1^*, which is often referred to as "Tsai's modulus". The formulas above, derived for arbitrary n, reduce directly to the known *DD* case for $n = 2$ (with $\phi_1 = \phi$, $\phi_2 = \psi$) and are consistent with published results for $[\pm\phi, \pm\psi]$ laminates.

An important design aspect of *n-D* laminates is the assumption of homogenisation: by repeating a basic $[\pm\phi_1, \ldots, \pm\phi_n]$ sub-laminate multiple times through the thickness, the effective properties of the laminate approach those of a homogeneous orthotropic plate. In the context of *DD* laminates ($n = 2$), Tsai notes that using a 4-ply repeating block (two $\pm\phi$ and two $\pm\psi$ plies) allows one to achieve a near-constant "master ply" stiffness with far fewer plies than a conventional 0/±45/90 layup. In fact, a homogenised *DD* laminate can retain roughly constant A_{ij} values even as plies are dropped, enabling tapering of thickness without abrupt in-plane stiffness changes. By contrast, a quad laminate requires a much thicker buildup (on the order of dozens of plies) before its properties stabilise. As n increases, the size of the repeating block (containing $2n$ plies for a symmetric stack) also increases, which can slow down the convergence to homogenised behaviour. Thus, there is a trade-off: although an *n*-double laminate with large n offers more flexibility in tailoring stiffness (and can theoretically approximate isotropy as $n \to \infty$), it may require more plies/repeats to achieve the same level of homogenisation as a smaller n design. In practice, *n-D* laminates for $n > 2$ have not seen widespread use; instead, the $n = 2$ case strikes a desirable balance between design simplicity and performance. Still, the generalisation to arbitrary n is conceptually useful and aligns with the classical laminate theory understanding that lamination parameters offer a compact representation of the in-plane and out-of-plane stiffness behaviour of a laminate, especially in the asymptotic limit of large ply counts.

Finally, by enforcing symmetry (mid-plane reflection) in an *n*-double laminate, the coupling matrix $[B]$ is zero (as assumed above), simplifying analysis and design. With $B = 0$, in-plane and bending responses are decoupled, and one can optimise the extensional stiffness $[A]$ independently of the flexural stiffness $[D]$. Moreover, a homogenised symmetric laminate allows ply drops to be done in balanced singles (removing one $\pm\phi_k$ pair at a time) without inducing coupling, which is an advantage over traditional designs that require removing

plies in mirror-symmetric pairs. This simplification is critical in wing panel optimisation, as highlighted by Shrivastava et al. [15], who demonstrated improved weight efficiency using DD building blocks under multiple load cases. In summary, the *n-D* laminate concept generalises the *DD* philosophy to an arbitrary number of angle-ply pairs, retaining the benefits of invariant-based stiffness descriptions and manufacturability considerations. Its theoretical formulation (Eq. (4)) leverages trace-normalised invariants to homogenise and simplify the stiffness analysis, while the practical design guidance (e.g., choosing $n = 2$ in most cases) stems from the desire to minimise complexity and maximise the homogenisation benefit. (For further reference, see Tsai's development of the *DD* family and invariant theory by Tsai & Melo [8], as well as recent studies extending *DD* concepts for advanced tailoring.)

In this study, we restrict the analysis to balanced and symmetric stacking sequences. While this limits the design space, the assumption is motivated by practical considerations in laminate design and manufacturing. Symmetry and balance help mitigate coupling between bending and extension, reduce residual stresses, and are widely adopted in the industry due to their certification history and simplified failure behaviour. However, it is acknowledged that these are sufficient, but not necessary, conditions for membrane/bending uncoupling. In particular, Quasi-Trivial (*QT*) stacks [3] represent a broader class of laminates that fulfil uncoupling and homogeneity conditions without relying on symmetry. The current framework may be extended in future work to include such generalised layups, potentially improving the optimality of the designs.

It is also acknowledged that, despite being symmetric and balanced, the *n-D* stacking sequences adopted in this study are not necessarily orthotropic in bending. This limitation is inherent to the *DD* formulation and has been rigorously demonstrated in the context of more general stacking theories, such as *QT* laminates and the polar method [3,5]. These frameworks enable a comprehensive representation of the in-plane and bending stiffness matrices, potentially leading to designs that are fully orthotropic or uncoupled in both *A* and *D* matrices. While our study prioritises structured and manufacturable designs, future work will aim to remove the balance and symmetry constraints to explore these broader classes of laminates.

While the trace of the in-plane stiffness matrix ($A_{11} + A_{22}$) provides a practical and intuitive indicator of in-plane stiffness, it is worth mentioning that it does not fully characterise the elastic symmetry of a 2D orthotropic or anisotropic laminate. In this regard, the polar method [1,4,6], offers a rigorous mathematical framework based on tensorial invariants. This method enables the classification of laminate stiffness according to symmetry classes (e.g., isotropic, orthotropic, monoclinic) and provides complete descriptors of the fourth-order in-plane elasticity tensor. Unlike the *DD* framework, which focuses on structural regularity and manufacturability, the polar formalism is particularly well-suited for theoretical design, inverse problems, and multi-scale optimisation strategies.

The membrane/bending *uncoupling condition*, mathematically defined as $B = 0$, and the *homogeneity condition*, which requires the in-plane stiffness matrix A and bending stiffness matrix D to have identical tensorial symmetries (i.e., $A^* = D^*$), are key requirements in many optimal laminate designs [3]. While these conditions can be exactly fulfilled in *QT* laminates with relatively few plies, the same is not generally true for *DD* or *n-D* stacks, unless a large number of plies is used and orientations are carefully chosen.

For example, the *QT* sequences

$$[\alpha/\beta/\alpha/\alpha/\alpha/\beta/\alpha] \quad \text{and} \quad [\alpha/\beta/\beta/\alpha/\beta/\alpha/\alpha/\beta]$$

where α and β are fibre angles, achieve both $B = 0$ and $A^* = D^*$ for arbitrary values of α and β in the range $[-90°, 90°]$. In contrast, *DD* designs impose stricter symmetry and angle repetition rules, making exact satisfaction of these conditions difficult in general. As such, while *DD* and *n-D* layouts offer excellent manufacturability and performance trade-offs, they should not be seen as universally optimal solutions in problems where lightweight design and elastic decoupling are critical. This highlights the importance of exploring more general stacking strategies, such as QT or polar-based designs, in future optimisation frameworks.

2.2. Linear buckling analysis

The description of the implemented formulation to calculate the critical linear buckling load is detailed in the Appendix.

2.3. The optimisation

The optimisation was conducted using a GA from the `pymoo` library [43]. The search space consisted of $n_{\text{var}} = 12$ variables, corresponding to a quarter of the 48-ply stacking sequence (the rest of the laminate is generated by enforcing symmetry and balance). The ply angle variables were restricted to integer values in the range 0°−90°, representing typical manufacturing constraints.

The GA was configured with the following parameters: a population size of 50, maximum number of generations $N_{\text{gen}} = 100$, and a random seed fixed at 1 for reproducibility. Integer-based random sampling was used to initialise the population. The Simulated Binary Crossover (SBX) operator was applied with a crossover probability of 1.0 and distribution index $\eta_c = 3.0$, followed by a polynomial mutation (PM) operator with mutation probability of 1.0 and mutation index $\eta_m = 3.0$. Both operators were configured to handle integer variables using the built-in rounding repair mechanism in `pymoo`. Duplicate individuals were eliminated to promote population diversity.

No explicit constraint handling was required within the GA since laminate balance and symmetry were enforced programmatically when reconstructing the full stacking sequence. The objective function was based on the inverse of the minimum between buckling load factor or failure load factor, consistent with the weighted aggregation strategy introduced by Haftka [44].

The optimisation problem can be described as follows:

$$\begin{aligned} \min_{\theta \in [0°, 90°]^n} \quad & f(\boldsymbol{\theta}) = \frac{1}{(1-p) \cdot \min\left(\lambda_{\text{cb}}(\boldsymbol{\phi}), \lambda_{\text{cs}}(\boldsymbol{\phi})\right)} \\ \text{subject to} \quad & \boldsymbol{\phi} = \text{Sym}\left(\text{Bal}\left(\boldsymbol{\theta} \cup (-\boldsymbol{\theta})\right)\right) \end{aligned} \tag{5}$$

The optimisation problem addressed in this study is characterised by a highly nonlinear, multimodal, and derivative-free objective function that depends on both the buckling and failure response of the laminate. Although the ply orientation angles are defined within a continuous range $[0°, 90°]$, the implemented genetic algorithm (GA) employs integer-based encoding with a resolution of 1°, while keeping balanced and symmetric stacking sequences. This representation enables the GA to efficiently explore the design space while naturally incorporating manufacturable angles, with buckling and failure constraints added through a penalty-based method.

It is acknowledged that metaheuristic algorithms such as GAs do not guarantee convergence to global or local optima. The solutions obtained herein are considered near-optimal, representing high-performance designs within the explored parameter space and algorithm settings.

3. Results and discussion

The benchmark study by Le Riche and Haftka [44] is considered, in which a symmetric laminated composite plate with 64 plies, simply supported along all four edges, is subjected to biaxial in-plane loading, as illustrated in Fig. 1. The stacking sequence is optimised to maximise the buckling load factor. In this case, the plate has dimensions $a = 508\,\text{mm}$ (20 in) and $b = 254\,\text{mm}$ (10 in), and is subjected to uniform in-plane loads of $N_x = N_y = 0.17513\,\text{N/m}$ (1 lb/in).

The material properties of the graphite-epoxy laminate used in this case, as reported in [44], are: longitudinal modulus $E_1 = 127.7$ GPa,

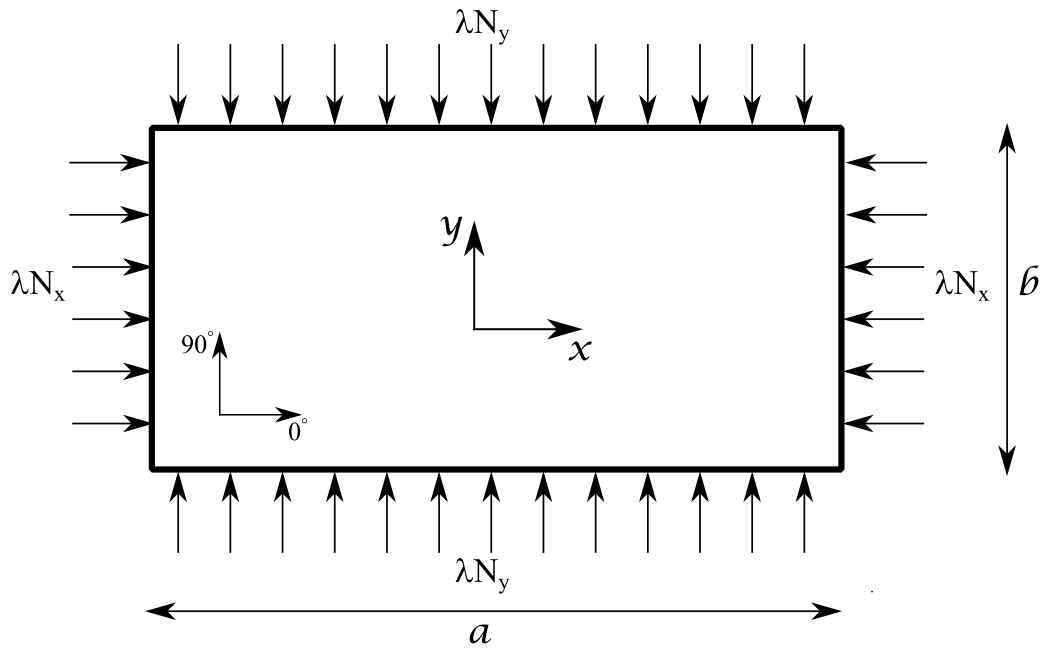

Fig. 1. Geometry, loads, and boundary conditions of the study case.

transverse modulus $E_2 = 13.0$ GPa, in-plane shear modulus $G_{12} = 6.41$ GPa, Poisson's ratio $\nu_{12} = 0.3$, and ply thickness $t_{\text{ply}} = 0.127$ mm. The ultimate strains are $\epsilon_1^{\text{ua}} = 0.008$, $\epsilon_2^{\text{ua}} = 0.029$, and $\gamma_{12}^{\text{ua}} = 0.015$.

To highlight the existence of multiple optima in laminate design, selected results from Le Riche and Haftka [44] are discussed. In their study, five different Quad stacking sequences for a symmetric 64-ply laminate, all evaluated using FE simulations, were shown to yield the same buckling load factor λ of 3973.01, despite having significantly different ply arrangements. This indicates that the buckling response is largely insensitive to the specific stacking sequence among these configurations. However, the corresponding failure load factors varied considerably, i.e., from 8935.74 to 14 205.18, revealing that the failure response is more sensitive to the laminate architecture. The detailed stacking sequences and load factors are omitted here for brevity, as they are already reported in the original publication (see Table 2 in [44]).

3.1. Direct stiffness matching approach

As proposed by Shrivastava et al. [15], the selection of equivalent *DD* laminates for Quad can be performed based on the best match of three terms of the thickness-normalised membrane stiffness matrix $[A^*] = (1/h)[A]$; based on the minimisation of the following error:

$$\begin{aligned}\mathcal{E} = &\left|\left(A_{11}^*\right)_{DD} - \left(A_{11}^*\right)_{LQL}\right| + \\ &\left|\left(A_{22}^*\right)_{DD} - \left(A_{22}^*\right)_{LQL}\right| + \\ &\left|\left(A_{66}^*\right)_{DD} - \left(A_{66}^*\right)_{LQL}\right|\end{aligned} \tag{6}$$

Although *DD* laminates can closely approximate target stiffness values using coarse angle discretisations (e.g., 1° steps), and achieve even better matching with finer resolution, this does not directly correlate with improved buckling performance. In Table 2, a stiffness-matching exercise is performed using 48-ply quasi-isotropic reference laminates from Le Riche and Haftka [44]. These results refer exclusively to conventional quad laminates optimised using the stiffness matching approach described in Ref. [15], and are reported here to highlight an important limitation: matching the A and D matrices does not necessarily predict buckling or failure loads accurately. This underscores the need for design frameworks, such as the proposed *n-D* approach, that consider the full coupling between geometry, stacking, and structural performance.

3.2. Convergence analysis

Fig. 2 presents the convergence behaviour of the GA for both the 48-layer and 64-layer laminate optimisation problems, considering variations in population size and number of generations. For the 48-layer case, subfigures (a) and (b) show that increasing the population size and the number of generations improves the convergence rate and the final buckling load factor, λ, up to a certain point. Specifically, a population size of 40 or 50 and a minimum of 60 generations appear sufficient to consistently reach the maximum load factor, suggesting a good trade-off between computational cost and performance.

A similar trend is observed for the 64-layer laminate in subfigures (c) and (d). The GA shows sensitivity to the choice of population size in early generations but quickly stabilises with larger populations. Notably, beyond 25 individuals and 40 generations, the differences in final λ become negligible, indicating convergence to a near-optimal layup. This behaviour demonstrates the robustness of the GA in handling high-dimensional stacking sequence optimisation problems and highlights the importance of proper tuning of algorithm parameters for efficient search.

3.3. Buckling optimisation

Table 3 presents the buckling and failure load factors (λ) obtained for a 48-layer composite laminate subjected to biaxial and uniaxial compression, considering different stacking sequence configurations (*n*-D layouts), aspect ratios (a/b), and boundary conditions (BC). The stacking sequences include traditional single-angle (*D*), double-angle (*DD*), and more multi-angle layouts (*DDD* and *DDDD*), with GA representing a completely unrestricted and unconstrained design where the GA selects arbitrary ply angles.

For both biaxial and uniaxial loadings, a clear trend is observed: increasing the freedom of ply orientations (i.e., moving from *D* to *DDDD*) generally improves both buckling and failure performance. This is especially evident in biaxial loading at low aspect ratios ($a/b = 0.5$), where the buckling load increases from 23 364 (*D*) to 27 484 (*DDDD*), and the failure load increases from 13 750 to 12 634. Interestingly, the best buckling performance is consistently achieved by the unrestricted GA layouts, though these do not always result in the best failure loads.

Table 2
Stiffness matching optimisation results: Optimised stacking sequences for buckling and failure loads allowing n-D layouts for a 48–layer laminate. All results are in terms of load factor (λ).

Layout	Stacking sequence (Quad)	Stacking sequence (Optimised)	Buckling load factor	Failure load factor	(ϵ)
D	$[90_2/\pm45_2/90_2/\pm45/90_2/\pm45_6]_s$	$[\pm54]_{24}$	9998.18	8876.36	(8.1×10^{-2})
	$[90_4/\pm45_4/90_2/\pm45/90_2/\pm45_3]_s$	$[\pm57]_{24}$	9997.60	9675.74	(8.8×10^{-2})
	$[\pm45_2/90_4/\pm45/90_2/\pm45_5/90_2/\pm45]_s$	$[\pm57]_{24}$	9976.58	9675.74	(8.8×10^{-2})
DD	$[90_2/\pm45_2/90_2/\pm45/90_2/\pm45_6]_s$	$[\pm40/\pm66]_{12}$	9998.18	8749.30	(5.8×10^{-3})
	$[90_4/\pm45_4/90_2/\pm45/90_2/\pm45_3]_s$	$[\pm41/\pm72]_{12}$	9997.60	9533.58	(1.9×10^{-3})
	$[\pm45_2/90_4/\pm45/90_2/\pm45_5/90_2/\pm45]_s$	$[\pm41/\pm72]_{12}$	9976.58	9533.58	(1.9×10^{-3})
DDD	$[90_2/\pm45_2/90_2/\pm45/90_2/\pm45_6]_s$	$[\pm37/\pm52/\pm71]_8$	9998.18	8799.94	(1.4×10^{-3})
	$[90_4/\pm45_4/90_2/\pm45/90_2/\pm45_3]_s$	$[\pm60/\pm72/\pm36]_8$	9997.60	9515.65	(4.2×10^{-16})
	$[\pm45_2/90_4/\pm45/90_2/\pm45_5/90_2/\pm45]_s$	$[\pm60/\pm72/\pm36]_8$	9976.58	9515.65	(2.5×10^{-16})
DDDD	$[90_2/\pm45_2/90_2/\pm45/90_2/\pm45_6]_s$	$[\pm45/\pm45/\pm45/90_2]_6$	9998.18	8786.63	(5.8×10^{-16})
	$[90_4/\pm45_4/90_2/\pm45/90_2/\pm45_3]_s$	$[\pm64/\pm82/\pm41/\pm42]_6$	9997.60	9515.48	(2.2×10^{-5})
	$[\pm45_2/90_4/\pm45/90_2/\pm45_5/90_2/\pm45]_s$	$[\pm64/\pm82/\pm41/\pm42]_6$	9976.58	9515.48	(2.2×10^{-5})

Note: $a = 20$ in., $b = 5$ in., $N_x = 1.0$ lb/in, $N_y = 0.5$ lb/in. The error ϵ quantifies the difference between the stiffness-matched and target designs.

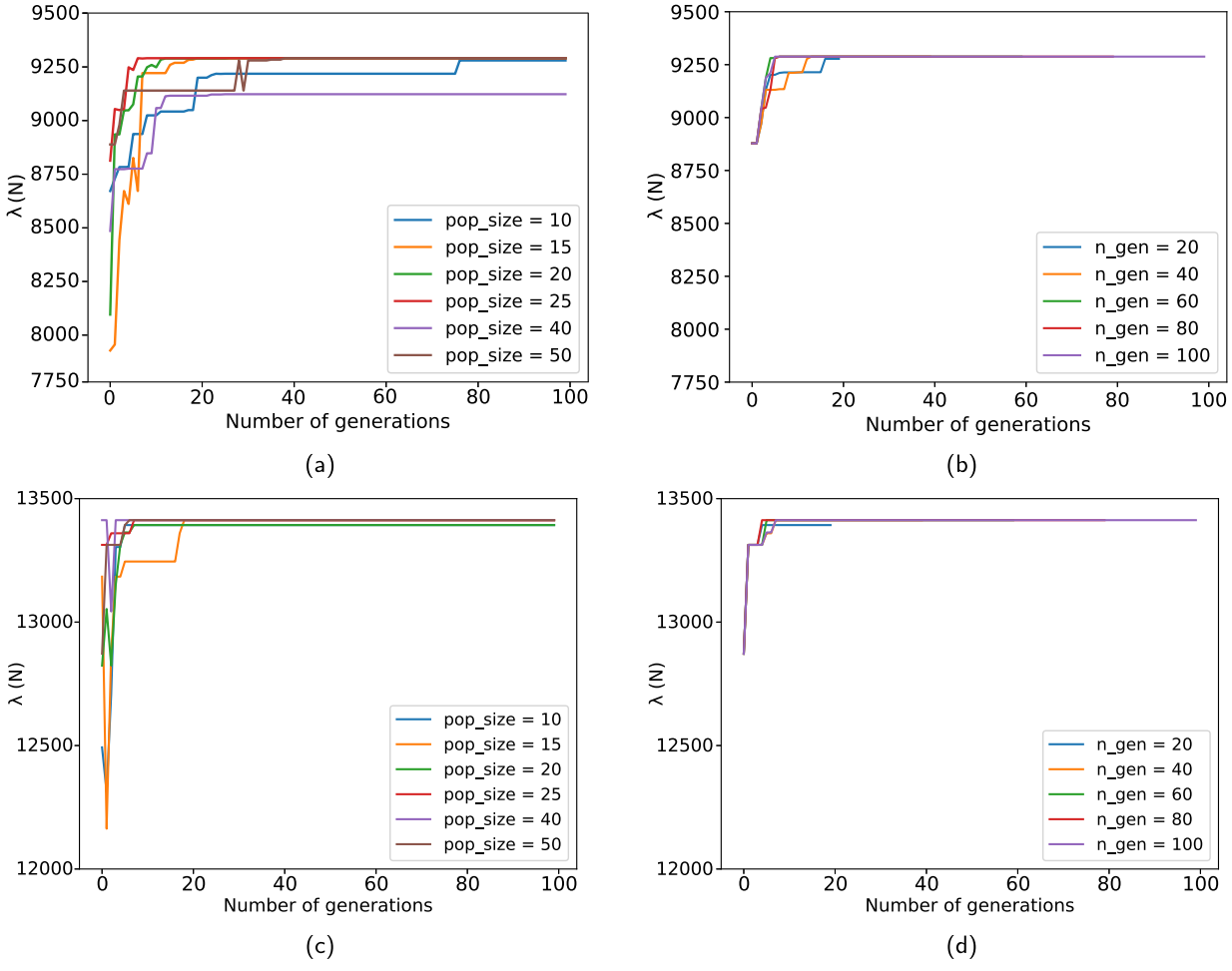

Fig. 2. Convergence analysis for the 48-layer laminate varying the (a) population size and (b) number of generations, and for the 64-layer laminate varying the (c) population size and (d) number of generations.

This highlights the trade-off between structural stiffness and failure strength that must be managed in laminate design.

Comparing the two boundary conditions reveals that uniaxial compression leads to higher buckling and failure loads across all configurations and stacking types. For instance, at $a/b = 0.5$, the GA layout under uniaxial compression yields a buckling load of 36 395 compared to 25 728 under biaxial loading—a relative increase of about 41%. This is consistent with the structural mechanics of plate buckling, where uniaxial loading permits higher critical loads due to less distributed compression.

The aspect ratio has a pronounced effect on both buckling and failure responses. In general, increasing the aspect ratio from $a/b = 0.5$ to 4.0 leads to a reduction in both buckling and failure loads for most configurations. However, the effect is more severe in configurations with limited design freedom (*D* and *DD*). In contrast, the *DDDD* and GA configurations exhibit more stable performance across the range of a/b

Table 3
Buckling and failure loads allowing *n-D* layouts for a 48-layer laminate. All results are in terms of load factor (λ).

BC	n-D	**a/b ratio**				
		0.5	1.0	2.0	3.0	4.0
		Buckling/Failure	Buckling/Failure	Buckling/Failure	Buckling/Failure	Buckling/Failure
Biaxial	Free	25,728/18,537	12,464/17,850	10,615/10,633	10,484/10,489	10,453/10,549
	D	23,364/13,750	10,247/9252	7467/14,101	7285/12,092	5562/11,795
	DD	23,893/15,424	10,829/14,713	8903/13,442	9341/12,424	8571/10,995
	DDD	24,907/10,804	11,663/11,084	9098/10,531	8792/11,041	7717/11,279
	DDDD	27,484/12,634	11,724/10,019	9102/10,151	9079/11,995	9291/11,931
Uniaxial	Free	36,395/23,679	16,881/16,880	16,863/16,865	16,679/16,693	16,724/16,727
	D	25,898/13,978	15,851/10,193	15,444/8588	16,170/8634	14,780/12,440
	DD	32,912/13,648	17,204/9553	16,180/11,342	15,487/10,298	16,105/10,211
	DDD	33,052/14,493	17,082/12,205	16,965/9371	17,530/9027	16,934/8804
	DDDD	30,801/10,797	17,339/8903	17,736/9015	16,793/10,830	16,693/10,258

ratios, demonstrating the robustness of highly flexible stacking designs to changes in geometry.

Although GA consistently provides the highest buckling loads, its failure loads are sometimes lower than those achieved with more structured *DDDD* layouts. For example, under uniaxial loading at $a/b = 2.0$, GA achieves a failure load of 16 865, while DDDD achieves 9015. However, the *DDDD* configuration achieves similar buckling performance (17 736 vs. 16 865) with a better failure-to-buckling ratio ($\lambda_{\text{failure}}/\lambda_{\text{buckling}}$), indicating a more balanced design. Thus, while GA offers maximum flexibility, structured multi-angle configurations like *DDDD* offer superior trade-offs for design scenarios where failure must be avoided.

The DD stacking concept proposed by Tsai is clearly extended and outperformed by the more generalised *DDD* and *DDDD* stacking patterns. This is evident in both loading scenarios and across all aspect ratios. For instance, at $a/b = 1.0$ under uniaxial loading, the DD configuration yields a buckling load of 17 204, while the *DDDD* achieves 17339. Although the improvement is marginal here, the trend becomes more significant at higher aspect ratios and in biaxial loading scenarios.

Overall, these results highlight the value of enabling richer stacking sequence layouts in laminate design. Not only do *DDD* and *DDDD* configurations outperform the traditional *D* and *DD* designs in terms of buckling and failure loads, but they also offer robustness across geometrical and loading variations, thus advancing the current state of the art in stacking sequence optimisation.

Table 4 summarises the buckling and failure load factors (λ) obtained for 64-layer composite laminates subjected to both biaxial and uniaxial compressive boundary conditions (BC), for a range of a/b aspect ratios. Compared to the 48-layer case (Table 3), these thicker laminates demonstrate notably higher structural performance across all stacking configurations, which is expected due to increased flexural stiffness. However, the *DDD* layout is no longer feasible for 64-ply laminates due to ply count constraints, and the comparison is therefore limited to *D*, *DD*, *DDDD*, and GA (free-angle) stacking sequences.

The comparative performance of *D*, *DD*, *DDDD*, and free-angled-constrained stacking sequences must be interpreted carefully. While free-angled-constrained layups offer more flexibility, they involve a larger number of design variables, increasing the risk of convergence to sub-optimal regions due to the multimodal nature of the problem. In contrast, *n-D* configurations with fewer angles may benefit from design regularity, better fibre alignment, and more efficient load transfer, especially under compressive loads. Although the free-angled-constrained solutions are not guaranteed to be globally optimal (due to the stochastic nature of the GA algorithm), they represent high-performing candidates obtained through extensive search. The superior performance of some structured stacks, despite their restricted design space, highlights the trade-off between freedom and robustness in stacking sequence design.

As in the 48-layer case, increasing the design freedom through more general stacking sequences (from *D* to *DDDD*) consistently improves performance across most load cases. For instance, under biaxial loading at $a/b = 0.5$, the buckling load improves from 41 870 (*D*) to 43 516 (*DD*) and then slightly decreases to 42 170 (*DDDD*). However, the failure load consistently increases from 16 516 (*D*) to 17 699 (*DDDD*), showing that more complex layups can better manage interlaminar stresses and delay failure. Interestingly, the GA layout, which is free from angular constraints, does not always outperform structured configurations. For example, under biaxial compression at $a/b = 1.0$, *DDDD* achieves a higher failure load (17 867) than GA (18 537), but GA underperforms in buckling (19 168 vs. 19 079 for *DDDD*). This suggests that, for 64-ply laminates, structured multi-angle sequences may offer a better balance of stiffness and strength than unconstrained optimisation.

Uniaxial compression again results in significantly higher buckling and failure loads compared to biaxial compression for all layouts. For example, under uniaxial loading at $a/b = 0.5$, the GA configuration yields a buckling load of 82 629, which is more than twice the corresponding value under biaxial loading (37 698). This trend is consistent across all a/b ratios and highlights the less demanding nature of uniaxial stability requirements in terms of load distribution.

As in the 48-ply case, increasing the a/b ratio generally reduces the buckling and failure loads. This trend is more pronounced in the *D* and *DD* layouts than in DDDD and GA. For instance, under biaxial loading using *DD*, buckling loads drop from 43 516 ($a/b = 0.5$) to 7226 ($a/b = 4.0$) — a reduction of over 80%. In contrast, *DDDD* exhibits a more gradual drop (from 42 170 to 11 440). The robustness of *DDDD* and GA configurations to changes in aspect ratio is advantageous in applications with geometrical variability or manufacturing tolerance considerations.

Although the GA layout often gives the highest buckling loads (e.g., 82 629 under uniaxial loading at $a/b = 0.5$), the *DDDD* configuration proves competitive, particularly in maintaining superior failure load performance with reduced design complexity. For example, under uniaxial compression at $a/b = 3.0$, *DDDD* achieves 35 065 in buckling and 16 225 in failure load, compared to GA's 28 164 and 28 164. This result supports the use of structured multi-angle designs over unconstrained solutions when balancing manufacturability, robustness, and performance.

The 64-layer results reinforce the findings from the 48-layer case but also demonstrate that the relative benefits of added stacking freedom saturate or slightly diminish as ply count increases. Structured layouts like *DD* and *DDDD* offer significant performance gains over traditional D laminates, and in many cases rival or exceed the performance of GA-derived designs, particularly for failure criteria. Moreover, the exclusion of DDD in the 64-ply case emphasises the need for discrete stacking options compatible with manufacturing constraints and ply symmetry.

In summary, *DDDD* stacking layouts offer an effective balance between structural performance, design robustness, and manufacturability for thick laminates, extending the benefits of Tsai's *DD* theory and offering a viable alternative to fully free-angle optimisations.

Table 4
Buckling and failure loads for *n-D* stacking configurations and free-angle-constrained designs in a 64-layer laminate under various aspect ratios. All results are in terms of load factor (λ).

BC	n-D	a/b ratio				
		0.5	1.0	2.0	3.0	4.0
		Buckling/Failure	Buckling/Failure	Buckling/Failure	Buckling/Failure	Buckling/Failure
Biaxial	GA	37,698/18,537	19,168/18,537	15,942/15,953	15,892/15,914	15,805/16,022
	D	41,870/16,516	19,835/16,763	9468/15,512	8368/17,185	8321/18,284
	DD	43,516/15,629	18,097/14,616	10,736/11,269	11,651/11,851	7226/12,562
	DDDD	42,170/15,432	18,990/17,679	15,078/9817	11,879/16,269	11,410/15,302
Uniaxial	GA	86,269/31,573	30,171/30,171	29,290/29,288	28,165/28,167	28,184/28,186
	D	62,690/17,188	35,661/17,181	34,737/15,299	36,694/12,020	33,129/15,299
	DD	64,191/15,460	35,636/16,924	34,359/14,942	36,717/13,802	35,797/13,880
	DDDD	77,395/19,859	31,358/17,447	34,557/15,218	35,065/16,225	30,000/16,995

3.4. Analysis of optimised n-d stacking sequences

The full stacking sequence for every optimisation case presented in Section 3.3 is detailed in Tables 5, 6, 7, 8. The results are interpreted by category, as follows:

Influence of layup complexity (D to DDDD): Across both ply counts, a clear progression is observed as the number of allowed ply orientations increases. *D* layouts produce uniform $[\pm\theta]_n$ configurations, while *DD*, *DDD*, and *DDDD* allow greater directional flexibility, significantly improving structural tailoring. Notably, DDDD layouts yield diverse angle sets, especially at high a/b ratios, while maintaining symmetry and manufacturability.

Biaxial compression: In the 48-ply case (Table 5), *DDDD* sequences range from $[\pm 18/\pm 18/\pm 18/\pm 18]_6$ at $a/b = 0.5$ to $[\pm 34/\pm 39/\pm 33/\pm 33]_6$ at $a/b = 4.0$. The 64-ply *DDDD* layups (Table 7) include wider angles (e.g., $\pm 82/\pm 49/\pm 49/\pm 75$) indicating enhanced orthotropy. GA solutions resemble these patterns, confirming that DDDD serves as a structured surrogate to unconstrained optimisation.

Uniaxial compression: Under uniaxial loading (Tables 6 and 8), optimal sequences favour low-angle plies aligned with the load direction. For instance, $[\pm 0]_{24}$ is optimal for D layout at $a/b = 0.5$. *DDDD* still provides angular variation (e.g., $\pm 34/\pm 37/\pm 37/\pm 35$) to control out-of-plane deformation and shear.

Effect of removing n–D restrictions: When the *n-D* constraints are relaxed (last row in Tables 5, 6, 7, 8), GA and *DDDD* solutions show greater angular variability, finely tuned to both stiffness and strength. However, this comes with decreased regularity, which may reduce robustness and complicate manufacturing. The structured *DDDD* designs offer nearly equivalent performance with improved practicality.

4. Discussion

This section presents a comprehensive analysis of the optimisation results obtained for 48- and 64-layer composite laminates under biaxial and uniaxial compressive loads. The effects of stacking sequence generalisation through *n-D* layouts (ranging from *D* to *DDDD*), loading condition, and aspect ratio (a/b) are examined with respect to both buckling and failure load factors. The derived findings from Tables 3, 4 are discussed next.

4.1. Stiffness matching and design generalisation

As presented in Table 2, stiffness matching was performed for 48-layer laminates using reference stacking sequences from Le Riche and Haftka [44]. Although *DD* laminates are capable of closely matching the in-plane stiffness using angle steps as coarse as 1°, the results reveal that stiffness matching alone does not correlate strongly with the buckling performance.

Although the proposed *n-D* configurations demonstrate a structured pathway to approximate reference stiffnesses using a small number of orientation angles, these stiffness-matched designs do not consistently translate into optimal buckling performance. This mismatch highlights a key limitation of stiffness matching when applied to a constrained subset of stacking sequences. As rigorously discussed in [45], the laminate feasibility domain in lamination parameter space is inherently non-convex, and matching theoretical stiffness matrices becomes increasingly difficult when the number of available orientation angles (n) is low. While the stiffness matching strategy remains a powerful tool in macroscopic laminate design, its accuracy and predictive capability are fundamentally limited unless the full diversity of stacking orientations is permitted. This supports the use of full buckling and failure evaluations in optimisation studies, particularly when the design space is intentionally reduced for manufacturability or robustness.

A visual representation of the optimisation results can be seen in Figs. 3, 4, 5, 6.

4.2. 48-Ply laminate: Buckling and failure under biaxial and uniaxial loads

Figs. 3 and 4 illustrate the optimisation outcomes for 48-ply laminates. Under biaxial loading (Fig. 3(a,b)), the buckling performance consistently improves from *D* to *DDDD* layouts across all aspect ratios. The *DDDD* configuration closely approximates the results of the unconstrained GA solution, especially at lower aspect ratios ($a/b = 0.5$–1.0), where buckling loads exceed 25 kN.

Similarly, for failure load (Fig. 3(c,d)), *DDDD* and GA solutions exhibit superior performance. At higher aspect ratios ($a/b > 2.0$), *DDDD* matches or outperforms GA in terms of failure load, suggesting its robustness and effectiveness as a manufacturable alternative.

Under uniaxial loading (Fig. 4(c,d)), overall load capacities increase, with buckling loads reaching 35 kN and failure loads over 20 kN. *DDDD* again performs competitively with GA, particularly in strength optimisation, offering near-optimal solutions with increased structural regularity and manufacturability.

4.3. 64-Ply laminate: Performance trends and limitations of DDD

Table 4 and Figs. 5–6 present the optimisation results for 64-layer laminates. Due to ply count limitations, the *DDD* layout was excluded in this case. Under biaxial compression, *DDDD* and GA deliver the highest buckling loads, approaching 38 kN. The failure loads reveal a similar trend: while GA achieves maximum buckling, *DDDD* offers higher or comparable failure load factors across most a/b ratios. This indicates that *DDDD* designs balance stiffness and strength better than unconstrained solutions, which may overfit to buckling alone.

For uniaxial loading, peak buckling loads approach 85 kN for GA solutions, with *DDDD* trailing closely behind. However, *DDDD* outperforms all structured layouts in failure resistance and, at times, even surpasses the GA design. This again demonstrates the *DDDD* ability of the layout to offer balanced optimisation across objectives.

Table 5
Optimised stacking sequences for biaxial compression load allowing *n*–D layouts for a 48–layer laminate with different a/b ratios.

n-D	a/b ratio	Angles
D	2.5/5	$[\pm 17]_{12_{sym}}$
	5/5	$[\pm 45]_{12_{sym}}$
	10/5	$[\pm 52]_{12_{sym}}$
	15/5	$[\pm 53]_{12_{sym}}$
	20/5	$[\pm 53]_{12_{sym}}$
DD	2.5/5	$[\pm 17/\pm 17]_{6_{sym}}$
	5/5	$[\pm 45/\pm 45]_{6_{sym}}$
	10/5	$[\pm 88/\pm 43]_{6_{sym}}$
	15/5	$[\pm 73/\pm 43]_{6_{sym}}$
	20/5	$[\pm 77/\pm 43]_{6_{sym}}$
DDD	2.5/5	$[\pm 17/\pm 17/\pm 17]_{4_{sym}}$
	5/5	$[\pm 45/\pm 45/\pm 45]_{4_{sym}}$
	10/5	$[\pm 56/\pm 90/\pm 39]_{4_{sym}}$
	15/5	$[\pm 56/\pm 84/\pm 39]_{4_{sym}}$
	20/5	$[\pm 56/\pm 90/\pm 39]_{4_{sym}}$
DDDD	2.5/5	$[\pm 18/\pm 18/\pm 18/\pm 18]_{3_{sym}}$
	5/5	$[\pm 45/\pm 45/\pm 45/\pm 45]_{3_{sym}}$
	10/5	$[\pm 43/\pm 43/\pm 87/\pm 89]_{3_{sym}}$
	15/5	$[\pm 77/\pm 74/\pm 42/\pm 44]_{3_{sym}}$
	20/5	$[\pm 34/\pm 39/\pm 33/\pm 33]_{3_{sym}}$
GA with free angles	2.5/5	$[\pm 7/\pm 38/\pm 8/\pm 3/\pm 15/\pm 1/\pm 61/\pm 54/\pm 49/\pm 21/\pm 67/\pm 42]_{sym}$
	5/5	$[\pm 45/\pm 45/\pm 45/\pm 45/\pm 45/\pm 45/\pm 45/\pm 45/\pm 44/\pm 44/\pm 46]_{sym}$
	10/5	$[\pm 69/\pm 63/\pm 63/\pm 64/\pm 76/\pm 56/\pm 58/\pm 57/\pm 17/\pm 21/\pm 15/\pm 16]_{sym}$
	15/5	$[\pm 62/\pm 62/\pm 62/\pm 59/\pm 63/\pm 69/\pm 61/\pm 59/\pm 23/\pm 8/\pm 4/\pm 5]_{sym}$
	20/5	$[\pm 64/\pm 64/\pm 61/\pm 65/\pm 60/\pm 76/\pm 55/\pm 79/\pm 8/\pm 16/\pm 16/\pm 4]_{sym}$

Table 6
Optimised stacking sequences for uniaxial compression load ($n_{yy} = 0$) allowing *n*–D layouts for a 48–layer laminate with different a/b ratios. Note that for cases with identical fibre angles (e.g., all 0°), differences in performance arise from the grouping and spatial distribution of plies across n-D directional blocks, not from fibre orientation alone.

n-D	a/b ratio	Angles
D	2.5/5	$[\pm 0]_{12_{sym}}$
	5/5	$[\pm 36]_{12_{sym}}$
	10/5	$[\pm 36]_{12_{sym}}$
	15/5	$[\pm 36]_{12_{sym}}$
	20/5	$[\pm 36]_{12_{sym}}$
DD	2.5/5	$[\pm 0/\pm 0]_{6_{sym}}$
	5/5	$[\pm 37/\pm 34]_{6_{sym}}$
	10/5	$[\pm 36/\pm 36]_{6_{sym}}$
	15/5	$[\pm 36/\pm 36]_{6_{sym}}$
	20/5	$[\pm 36/\pm 36]_{6_{sym}}$
DDD	2.5/5	$[\pm 0/\pm 0/\pm 0]_{4_{sym}}$
	5/5	$[\pm 36/\pm 36/\pm 36]_{4_{sym}}$
	10/5	$[\pm 36/\pm 36/\pm 36]_{4_{sym}}$
	15/5	$[\pm 36/\pm 36/\pm 36]_{4_{sym}}$
	20/5	$[\pm 35/\pm 37/\pm 35]_{4_{sym}}$
DDDD	2.5/5	$[\pm 0/\pm 0/\pm 0/\pm 0]_{3_{sym}}$
	5/5	$[\pm 36/\pm 36/\pm 36/\pm 36]_{3_{sym}}$
	10/5	$[\pm 36/\pm 35/\pm 36/\pm 36]_{3_{sym}}$
	15/5	$[\pm 38/\pm 33/\pm 34/\pm 35]_{3_{sym}}$
	20/5	$[\pm 34/\pm 37/\pm 37/\pm 35]_{3_{sym}}$
GA with free angles	2.5/5	$[\pm 1/\pm 1/\pm 0/\pm 0/\pm 1/\pm 0/\pm 0/\pm 31/\pm 0/\pm 0/\pm 6/\pm 0]_{sym}$
	5/5	$[\pm 43/\pm 41/\pm 43/\pm 38/\pm 18/\pm 11/\pm 10/\pm 8/\pm 7/\pm 7/\pm 7/\pm 7]_{sym}$
	10/5	$[\pm 44/\pm 43/\pm 32/\pm 39/\pm 25/\pm 25/\pm 9/\pm 6/\pm 6/\pm 6/\pm 6/\pm 6]_{sym}$
	15/5	$[\pm 45/\pm 42/\pm 47/\pm 6/\pm 18/\pm 31/\pm 9/\pm 3/\pm 1/\pm 1/\pm 1/\pm 1]_{sym}$
	20/5	$[\pm 46/\pm 49/\pm 44/\pm 45/\pm 9/\pm 15/\pm 4/\pm 4/\pm 1/\pm 0/\pm 0/\pm 0]_{sym}$

Table 7
Optimised stacking sequences for biaxial compression load allowing *n*–D layouts for a 64–layer laminate with different a/b ratios.

n-D	a/b ratio	Angles
D	2.5/5	$[\pm 30]_{16_{sym}}$
	5/5	$[\pm 34]_{16_{sym}}$
	10/5	$[\pm 61]_{16_{sym}}$
	15/5	$[\pm 58]_{16_{sym}}$
	20/5	$[\pm 59]_{16_{sym}}$
DD	2.5/5	$[\pm 30/\pm 30]_{8_{sym}}$
	5/5	$[\pm 34/\pm 34]_{8_{sym}}$
	10/5	$[\pm 50/\pm 68]_{8_{sym}}$
	15/5	$[\pm 49/\pm 76]_{8_{sym}}$
	20/5	$[\pm 75/\pm 50]_{8_{sym}}$
DDDD	2.5/5	$[\pm 1/\pm 89/\pm 73/\pm 17]_{4_{sym}}$
	5/5	$[\pm 10/\pm 46/\pm 61/\pm 56]_{4_{sym}}$
	10/5	$[\pm 57/\pm 62/\pm 50/\pm 61]_{4_{sym}}$
	15/5	$[\pm 88/\pm 71/\pm 48/\pm 48]_{4_{sym}}$
	20/5	$[\pm 82/\pm 49/\pm 49/\pm 75]_{4_{sym}}$
GA with free angles	2.5/5	$[\pm 61/\pm 25/\pm 68/\pm 77/\pm 89/\pm 40/\pm 83/\pm 35/\pm 28/\pm 3/\pm 59/\pm 28/\pm 2/\pm 16/\pm 33/\pm 73]_{sym}$
	5/5	$[\pm 55/\pm 26/\pm 48/\pm 35/\pm 21/\pm 79/\pm 40/\pm 16/\pm 66/\pm 71/\pm 1/\pm 87/\pm 11/\pm 82/\pm 42/\pm 43]_{sym}$
	10/5	$[\pm 86/\pm 69/\pm 73/\pm 90/\pm 82/\pm 88/\pm 63/\pm 79/\pm 57/\pm 42/\pm 36/\pm 17/\pm 2/\pm 4/\pm 2/\pm 1]_{sym}$
	15/5	$[\pm 72/\pm 74/\pm 75/\pm 77/\pm 81/\pm 72/\pm 64/\pm 56/\pm 62/\pm 54/\pm 29/\pm 17/\pm 15/\pm 4/\pm 0/\pm 0]_{sym}$
	20/5	$[\pm 87/\pm 83/\pm 72/\pm 69/\pm 78/\pm 69/\pm 65/\pm 59/\pm 56/\pm 30/\pm 26/\pm 22/\pm 18/\pm 8/\pm 6/\pm 6]_{sym}$

Table 8
Optimised stacking sequences for uniaxial compression load ($n_{yy} = 0$) allowing *n*–D layouts for a 64–layer laminate with different a/b ratios.

n-D	a/b ratio	Angles
D	2.5/5	$[\pm 0]_{16_{sym}}$
	5/5	$[\pm 12]_{16_{sym}}$
	10/5	$[\pm 20]_{16_{sym}}$
	15/5	$[\pm 21]_{16_{sym}}$
	20/5	$[\pm 20]_{16_{sym}}$
DD	2.5/5	$[\pm 0/\pm 0]_{8_{sym}}$
	5/5	$[\pm 13/\pm 13]_{8_{sym}}$
	10/5	$[\pm 20/\pm 20]_{8_{sym}}$
	15/5	$[\pm 22/\pm 22]_{8_{sym}}$
	20/5	$[\pm 20/\pm 20]_{8_{sym}}$
DDDD	2.5/5	$[\pm 0/\pm 0/\pm 0/\pm 0]_{4_{sym}}$
	5/5	$[\pm 12/\pm 13/\pm 11/\pm 11]_{4_{sym}}$
	10/5	$[\pm 15/\pm 21/\pm 15/\pm 20]_{4_{sym}}$
	15/5	$[\pm 20/\pm 20/\pm 20/\pm 21]_{4_{sym}}$
	20/5	$[\pm 16/\pm 18/\pm 16/\pm 22]_{4_{sym}}$
GA with free angles	2.5/5	$[\pm 0/\pm 0/\pm 0/\pm 0/\pm 0/\pm 0/\pm 1/\pm 0/\pm 0/\pm 1/\pm 0/\pm 0/\pm 0/\pm 0/\pm 1/\pm 0]_{sym}$
	5/5	$[\pm 10/\pm 18/\pm 25/\pm 8/\pm 2/\pm 1/\pm 2/\pm 7/\pm 11/\pm 1/\pm 0/\pm 0/\pm 0/\pm 0/\pm 0/\pm 0]_{sym}$
	10/5	$[\pm 17/\pm 8/\pm 76/\pm 10/\pm 1/\pm 0/\pm 0/\pm 0/\pm 2/\pm 0/\pm 0/\pm 0/\pm 2/\pm 0/\pm 1/\pm 0]_{sym}$
	15/5	$[\pm 19/\pm 39/\pm 2/\pm 88/\pm 0/\pm 1/\pm 1/\pm 0/\pm 1/\pm 1/\pm 0/\pm 0/\pm 58/\pm 0/\pm 1/\pm 1]_{sym}$
	20/5	$[\pm 24/\pm 16/\pm 55/\pm 16/\pm 9/\pm 10/\pm 2/\pm 3/\pm 1/\pm 1/\pm 1/\pm 1/\pm 1/\pm 2/\pm 1/\pm 4]_{sym}$

An interesting observation is seen for the 64-ply laminate with an aspect ratio of $a/b = 0.5$, as shown in Table 6. Although the plies in all *n-D* configurations at $a/b = 0.5$ are oriented at 0°, the differences in performance arise from how the plies are grouped into directional blocks. For instance, *DDDD* uses four distinct blocks of [±0°], each repeated three times, resulting in a different through-thickness architecture and laminate stiffness distribution compared to the single-block layout in D. These differences affect buckling and failure loads despite the shared fibre angle.

4.4. Implications for laminate design

Across all studied cases, increasing the a/b ratio leads to lower buckling and failure loads, with this trend being more pronounced in simpler layouts such as *D* and *DD*. In contrast, *DDDD* and GA-optimised configurations demonstrate greater resilience to geometric variations. Among them, the *DDDD* layout offers a compelling compromise: it preserves most of the structural benefits of the GA designs while maintaining a high degree of regularity and manufacturability. These findings reinforce the extension of Tsai's *DD* theory into a broader *n*-D stacking framework, capable of capturing advanced laminate behaviours while respecting practical design constraints.

4.5. Polar plot analysis of optimised stacking sequences

The polar plots in Figs. 7 and 8 illustrate how the optimal fibre angle distributions evolve as the design transitions from a restricted layout (*D*) to fully free-angle (GA) stacking. Each subplot corresponds to a specific aspect ratio (a/b) and layout type. The angle diversity reflects the attempt of the laminate to balance stiffness and strength under given boundary and loading conditions.

Biaxial compression (48- and 64-layer laminates), Fig. 7 :. Under biaxial loading, *D* layouts are highly constrained, typically clustering around ±45° due to the need for symmetric in-plane stiffness. *DD* layouts also tend to favour ±45° as the dominant angle, with slight variations

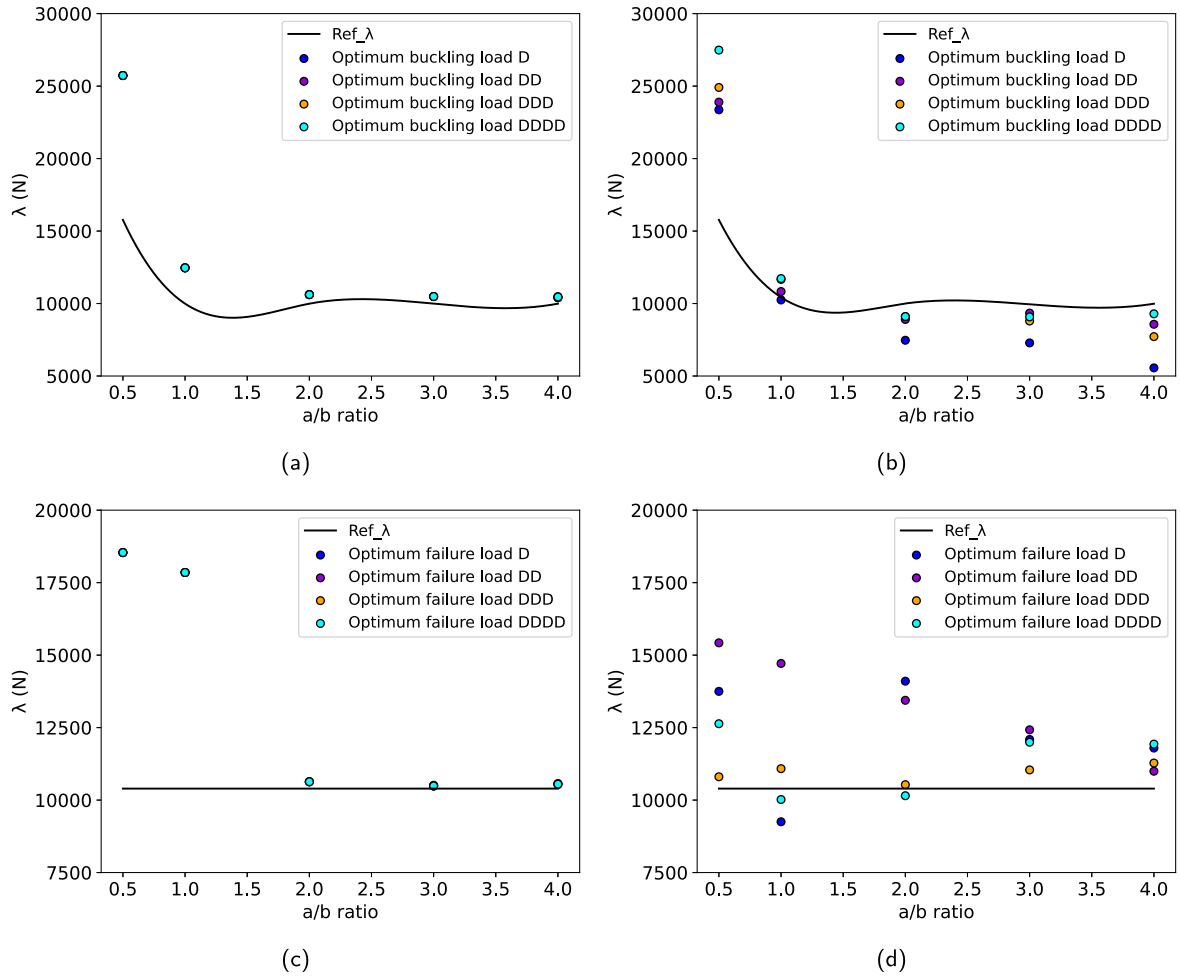

Fig. 3. Optimisation results for the 48-layer laminates under biaxial loading for buckling load factor (a) without angle restriction and (b) with *n-D* restriction; and for failure load factor (c) without angle restriction and (d) with *n-D* restriction.

(e.g., ±30° or ±60°) emerging at higher a/b ratios to adapt to directional buckling effects.

As the layout generalises to *DDD* and *DDDD*, broader angle sets appear, particularly in *DDDD*, where fibre angles span ±15° to ±60°, enabling tailored stiffness for complex buckling modes. GA solutions show smooth, continuous distributions including intermediate angles like ±18°, ±33°, and ±57°, optimised for precise modal control. *DDDD* approximates GA performance closely, while preserving structural regularity.

Uniaxial compression (48- and 64-layer laminates), Fig. 8 :. In contrast to the biaxial case, uniaxial compression results reveal a strong alignment of plies along the load axis. *D* and *DD* layouts cluster tightly around ±0°–±30°, maximising axial stiffness. *DDDD* layouts still favour low angles but introduce moderate diversity (e.g., ±10°, ±20°, ±35°) to account for out-of-plane stability and strength.

GA solutions show slightly skewed but broad angular distributions, balancing load alignment and shear resistance. *DDDD* proves particularly effective, avoiding over-alignment while still targeting axial performance.

Based on the qualitative assessment of the fibre distributions presented in Table 9, overall, *DDDD* provides structured angular diversity with performance comparable to GA. For biaxial designs, it offers modal robustness and shear-tailored stiffness. For uniaxial designs, it prevents over-alignment and enhances failure resistance. These results advocate for generalised *n-D* strategies as practical alternatives to fully free-angle designs, balancing manufacturability and high structural performance.

Table 9
Qualitative comparison of optimal fibre angle distributions under biaxial and uniaxial compression for different stacking layout strategies.

Observation	Biaxial	Uniaxial
Low-angle dominance	Weak (±45° typical)	Strong (±0°–±30°)
Angular diversity increases with layout freedom	Yes	Yes
DDDD mimics GA performance	Yes	Yes
Higher a/b leads to more spread	Strong	Mild
GA is smooth, *DDDD* is grouped	Yes	Yes

4.6. Limitations

The present work has the following limitations:

- The implemented finite element model is ready for use for linear buckling analysis;
- Geometric imperfections are not considered, although they can be considered not relevant for plates;
- As mentioned, the *DDDD* layout does not apply to the 64-ply laminate; and
- While a direct numerical comparison with prior *DD* laminate designs would be valuable, such benchmarks were not included here due to differing problem formulations, material systems, and load cases. The present study instead focuses on systematically

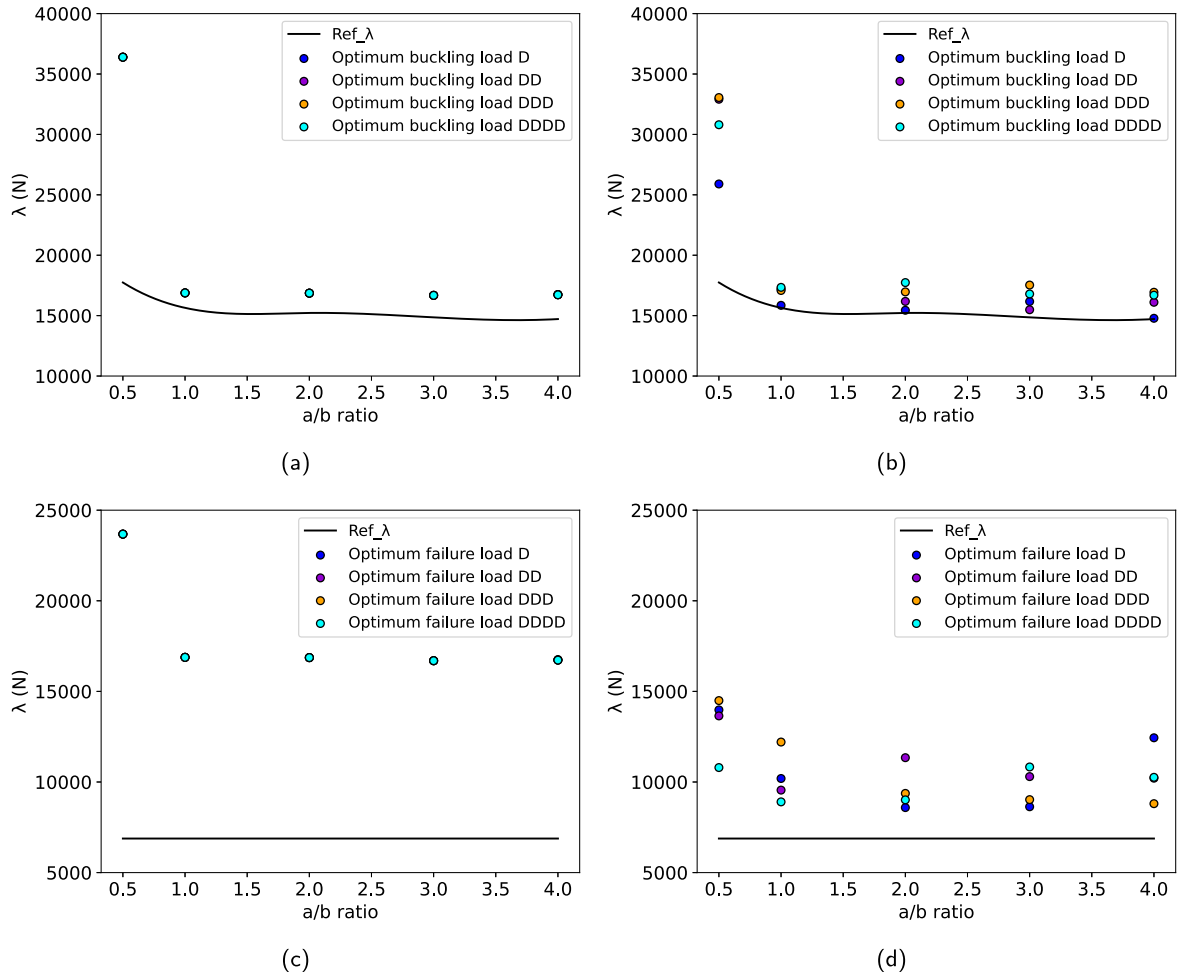

Fig. 4. Optimisation results for the 48-layer laminates under uniaxial loading for buckling load factor (a) without angle restriction and (b) with *n-D* restriction; and for failure load factor (c) without angle restriction and (d) with *n-D* restriction.

evaluating the influence of the number of directional blocks under consistent modelling assumptions. Future work will consider direct benchmarking for specific industrial case studies.

- The reliance on parameter tuning in metaheuristic algorithms can be a limitation in terms of robustness and generalisability. As such, parameter-free or self-adaptive strategies, such as the discrete Jaya algorithm (DJAYA) [46], represent promising alternatives for future investigations of *n-D* laminate optimisation.
- It must be noted that all optimal solutions presented herein are constrained to be symmetric and balanced. While this enhances manufacturability, it limits the potential to explore laminates that exhibit full orthotropy or isotropy in both membrane and bending behaviour. Such configurations may be better captured using unconstrained optimisation approaches such as the polar method or QT frameworks.

5. Conclusions

This study has presented a generalisation of Tsai's Double-Double (*DD*) laminate theory by introducing the concept of *n-Double* (*n-D* stacking layouts for composite laminates). A metaheuristic genetic algorithm was used to optimise the laminates for buckling and failure factors. By systematically evaluating the performance of *D*, *DD*, *DDD*, and *DDDD* stacking configurations under both biaxial and uniaxial compressive loads, across a range of aspect ratios, several key conclusions can be drawn:

- The proposed *n-D* approach significantly expands the composite design space by enabling greater directional tailoring while maintaining manufacturability through grouped ply orientations;
- *DDDD* configurations consistently outperform *D* and *DD* designs in both buckling and failure performance. In many cases, *DDDD* achieves near-identical results to free-angle GA-based optimisations, especially in strength-dominated scenarios.
- Under biaxial compression, *DDDD* and GA layouts introduce broad fibre angle distributions, providing modal robustness and optimised shear-stiffness combinations. For uniaxial compression, both favour low-angle plies, but *DDDD* avoids over-alignment and offers improved failure tolerance.
- Polar plots reveal that *DDDD* designs provide a structured yet flexible alternative to GA layouts, balancing optimal performance with practical manufacturability by limiting angular scatter and maintaining directional consistency.
- The findings advocate for the adoption of *n-D* stacking strategies in real-world composite structure design, offering a strong trade-off between performance, robustness, and production feasibility—especially critical in aerospace and advanced structural applications.

While this study employed a scalarised single-objective formulation to balance buckling and failure performance, future work will explore the use of multi-objective genetic algorithms (e.g., NSGA-II or NSGA-III) to generate Pareto fronts of optimal stacking sequences. This would enable a more comprehensive trade-off analysis and greater flexibility for application-specific laminate design.

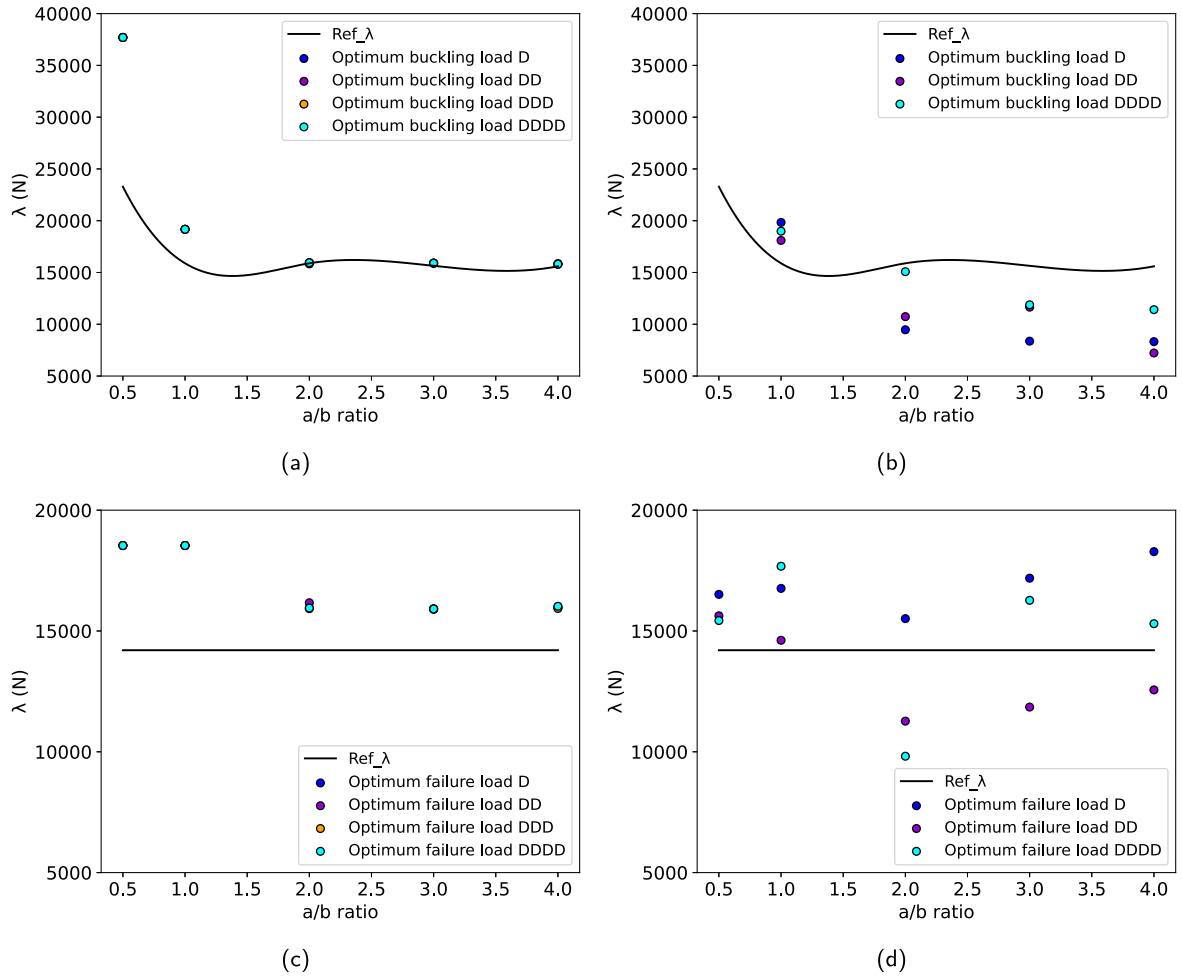

Fig. 5. Optimisation results for the 64-layer laminates under biaxial loading for buckling load factor (a) without angle restriction and (b) with *n-D* restriction; and for failure load factor (c) without angle restriction and (d) with *n-D* restriction.

The proposed *n-D* stacking design strategy offers a structured and manufacturable extension of the *DD* framework. However, the imposed constraints of symmetry and balance restrict the solution space and prevent exploration of general anisotropic designs that may provide better membrane–bending decoupling or stiffness tailoring. Future work will aim to relax these constraints and integrate more general formalisms such as polar-based invariants and multiscale optimisation. Additionally, although stiffness matching has been widely used as a surrogate for structural performance prediction, our results reinforce its limitations when only a small number of ply orientations are available. This does not undermine the theoretical foundation of lamination parameter-based design; rather, it reflects the geometric and non-convex nature of the feasible domain.

In conclusion, the generalised *n-D* design framework bridges the gap between conventional rule-based layups and unrestricted free-angle designs, opening new avenues for laminate optimisation that are both high-performing and industry-ready. Future research will focus on extending the optimisation framework in three key directions. First, a comparative analysis will be undertaken to evaluate alternative optimisation strategies, including parameter-free algorithms (e.g., DJAYA), differential evolution (DE), covariance matrix adaptation (CMA-ES), and gradient-based methods with filtering, to assess their suitability for *n-D* laminate design. Second, the formulation will be expanded to explicitly consider the post-buckling regime, where directional stacking strategies could be tailored to enhance load redistribution and energy absorption. Finally, practical integration with manufacturing processes will be pursued, including embedding constraints from automated fibre placement (AFP) and exploring the feasibility of fabricating *n-D* laminates through continuous fibre 3D printing technologies.

CRediT authorship contribution statement

José Humberto S. Almeida Jr.: Writing – original draft, Supervision, Software, Resources, Methodology, Formal analysis, Conceptualization. **Emilia Balonek:** Visualization, Formal analysis. **Saullo G.P. Castro:** Writing – original draft, Visualization, Software, Methodology, Formal analysis, Conceptualization.

Declaration of competing interest

The authors declare that they have no known competing financial interests or personal relationships that could have appeared to influence the work reported in this paper.

Acknowledgements

HA has received funding from the Research Council of Finland under grant number 364167.

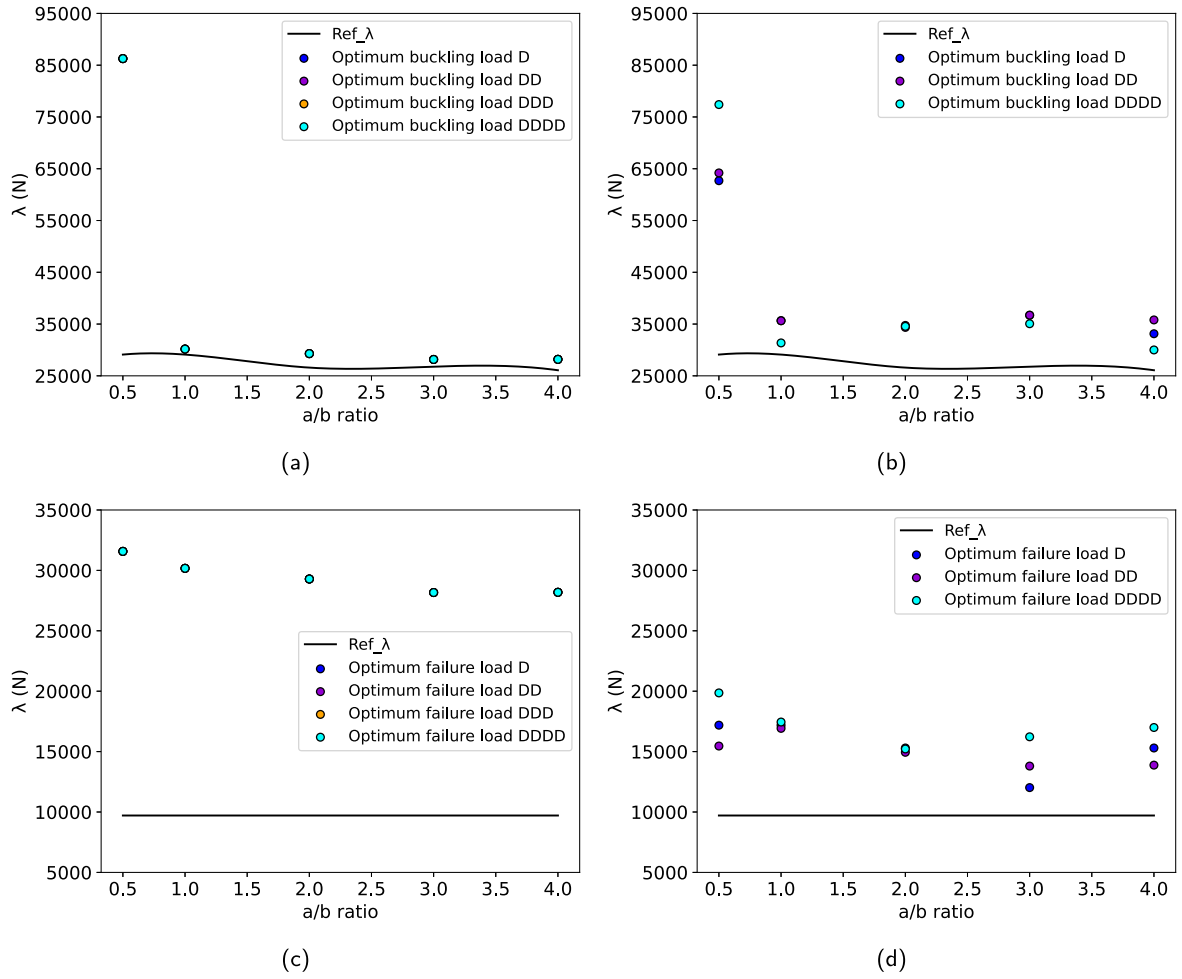

Fig. 6. Optimisation results for the 64-layer laminates under uniaxial loading for buckling load factor (a) without angle restriction and (b) with *n-D* restriction; and for failure load factor (c) without angle restriction and (d) with *n-D* restriction.

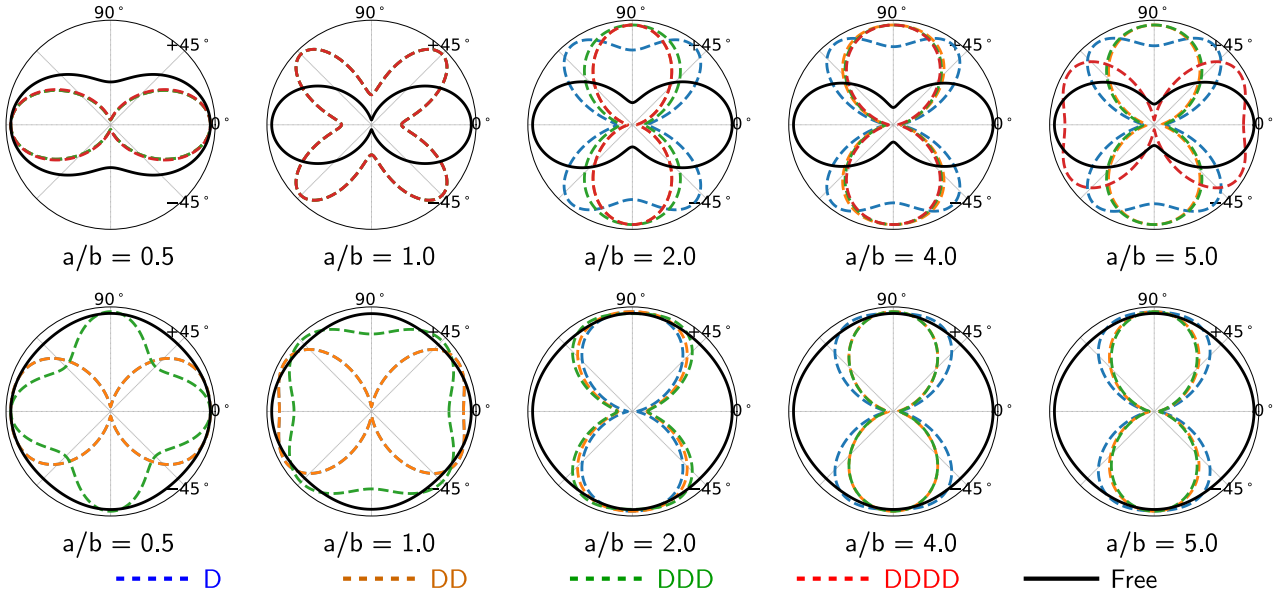

Fig. 7. Polar plots for all optimised stacking sequences under biaxial compression.

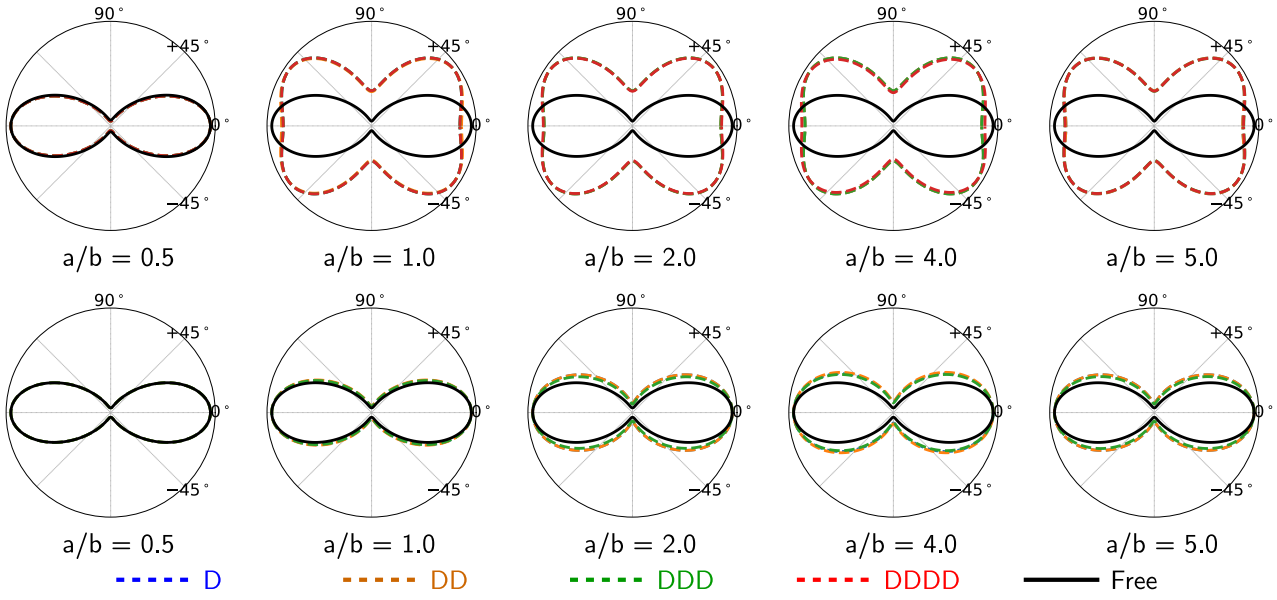

Fig. 8. Polar plots for all optimised stacking sequences under uniaxial compression.

Appendix. Linear buckling analysis calculation

Assuming equivalent single-layer theory [47,48], the total potential energy functional for one finite element ϕ_e can be expressed as:

$$\phi_e = \frac{1}{2}\int_{y=y_1}^{y_4}\int_{x=x_1}^{x_2} (\boldsymbol{N}\boldsymbol{\varepsilon} + \boldsymbol{M}\boldsymbol{\kappa})\, dxdy \tag{7}$$

where the membrane forces are $\boldsymbol{N} = \{N_{xx}, N_{yy}, N_{xy}\}^\top$ and the distributed moments are $\boldsymbol{M} = \{M_{xx}, M_{yy}, M_{xy}\}^\top$. The integration limits $x_1 \le x \le x_2$ and $y_1 \le y \le y_4$ define the domain of one rectangular finite element Ω_e. The membrane $\boldsymbol{\varepsilon}$ and rotational $\boldsymbol{\kappa}$ strains are assumed to follow von Kármán kinematics, also referred to in the literature as Donnell-type [49,50] or Kirchhoff–Love non-linear equations, given by:

$$\boldsymbol{\varepsilon} = \begin{Bmatrix} \varepsilon_{xx} \\ \varepsilon_{yy} \\ \gamma_{xy} \end{Bmatrix} = \begin{Bmatrix} u_{,x} + \frac{1}{2}w_{,x}^2 \\ v_{,y} + \frac{1}{2}w_{,y}^2 \\ u_{,y} + v_{,x} + w_{,x}w_{,y} \end{Bmatrix}$$
$$\boldsymbol{\kappa} = \begin{Bmatrix} \kappa_{xx} \\ \kappa_{yy} \\ \kappa_{xy} \end{Bmatrix} = \begin{Bmatrix} -w_{,xx} \\ -w_{,yy} \\ -2w_{,xy} \end{Bmatrix} \tag{8}$$

with $(\cdot)_{,x} = \partial(\cdot)/\partial x$ used as a compact notation for partial derivatives. At the bifurcation point, the following state of equilibrium exists, considering all n_e elements:

$$\delta\phi = \sum_{e=1}^{n_e}\delta\phi_e = \sum_{e=1}^{n_e}\int_{\Omega_e} \left(\boldsymbol{N}^\top\delta\boldsymbol{\varepsilon} + \boldsymbol{M}^\top\delta\boldsymbol{\kappa}\right) d\Omega_e = 0 \tag{9}$$

Expressing the displacements u, v, w within one element in terms of nodal coordinates $\boldsymbol{u}_e$ leads to: $u = \boldsymbol{S}^u\boldsymbol{u}_e$, $v = \boldsymbol{S}^v\boldsymbol{u}_e$, $w = \boldsymbol{S}^w\boldsymbol{u}_e$; such that $\delta\boldsymbol{\varepsilon}$ and $\delta\boldsymbol{\kappa}$ can be calculated as:

$$\delta\boldsymbol{\varepsilon} = \begin{bmatrix} \boldsymbol{S}^u_{,x} + w_{,x}\boldsymbol{S}^w_{,x} \\ \boldsymbol{S}^v_{,y} + w_{,y}\boldsymbol{S}^w_{,y} \\ \boldsymbol{S}^u_{,y} + \boldsymbol{S}^v_{,x} + w_{,x}\boldsymbol{S}^w_{,y} + w_{,y}\boldsymbol{S}^w_{,x} \end{bmatrix}\delta\boldsymbol{u}_e$$
$$\delta\boldsymbol{\kappa} = \begin{bmatrix} -\boldsymbol{S}^w_{,xx} \\ -\boldsymbol{S}^w_{,yy} \\ -2\boldsymbol{S}^w_{,xy} \end{bmatrix}\delta\boldsymbol{u}_e \tag{10}$$

where the partial derivatives of $\boldsymbol{S}^{u,v,w}$ are directly calculated from the shape functions of the BFSC element [51] in terms of the natural coordinates ξ, η, using the following Jacobian relations $\frac{\partial}{\partial x} = \frac{\ell_x}{2}\frac{\partial}{\partial\xi}$ and $\frac{\partial}{\partial y} = \frac{\ell_y}{2}\frac{\partial}{\partial\eta}$.

The neutral equilibrium criterion also requires that $\delta^2\phi_e = 0$ [52], such that, from Eq. (9):

$$\delta^2\phi = \sum_{e=1}^{n_e}\delta^2\phi_e = \sum_{e=1}^{n_e}\left[\int_{\Omega_e}\left(\delta\boldsymbol{N}^\top\delta\boldsymbol{\varepsilon} + \delta\boldsymbol{M}^\top\delta\boldsymbol{\kappa}+\right) d\Omega_e + \int_{\Omega_e}\left(\boldsymbol{N}^\top\delta^2\boldsymbol{\varepsilon} + \boldsymbol{M}^\top\delta^2\boldsymbol{\kappa}+\right) d\Omega_e\right] = 0 \tag{11}$$

The first integral of Eq. (11) becomes the constitutive stiffness matrix of the element, calculated using the constitutive relations from classical laminated plate theory [48]:

$$\delta\boldsymbol{N} = \boldsymbol{A}\delta\boldsymbol{\varepsilon} + \boldsymbol{B}\delta\boldsymbol{\kappa}$$
$$\delta\boldsymbol{M} = \boldsymbol{B}\delta\boldsymbol{\varepsilon} + \boldsymbol{D}\delta\boldsymbol{\kappa}$$

Note that the geometric non-linearity appears in the constitutive stiffness matrix due to $w_{,x}, w_{,y}, w_{,xy}$ in Eq. (10). Therefore, the linear constitutive stiffness matrix of a finite element $\boldsymbol{K}_e$ is calculated by assuming $w_{,x}, w_{,y}, w_{,xy} = 0$, leading to a 40×40 matrix:

$$\begin{aligned}\boldsymbol{K}_e = \iint_{xy} &\begin{bmatrix} \boldsymbol{S}^u_{,x} \\ \boldsymbol{S}^v_{,y} \\ \boldsymbol{S}^u_{,y} + \boldsymbol{S}^v_{,x} \end{bmatrix}^\top \boldsymbol{A} \begin{bmatrix} \boldsymbol{S}^u_{,x} \\ \boldsymbol{S}^v_{,y} \\ \boldsymbol{S}^u_{,y} + \boldsymbol{S}^v_{,x} \end{bmatrix} \\ &+ \begin{bmatrix} \boldsymbol{S}^u_{,x} \\ \boldsymbol{S}^v_{,y} \\ \boldsymbol{S}^u_{,y} + \boldsymbol{S}^v_{,x} \end{bmatrix}^\top \boldsymbol{B} \begin{bmatrix} -\boldsymbol{S}^w_{,xx} \\ -\boldsymbol{S}^w_{,yy} \\ -2\boldsymbol{S}^w_{,xy} \end{bmatrix} \\ &+ \begin{bmatrix} -\boldsymbol{S}^w_{,xx} \\ -\boldsymbol{S}^w_{,yy} \\ -2\boldsymbol{S}^w_{,xy} \end{bmatrix}^\top \boldsymbol{B} \begin{bmatrix} \boldsymbol{S}^u_{,x} \\ \boldsymbol{S}^v_{,y} \\ \boldsymbol{S}^u_{,y} + \boldsymbol{S}^v_{,x} \end{bmatrix} \\ &+ \begin{bmatrix} -\boldsymbol{S}^w_{,xx} \\ -\boldsymbol{S}^w_{,yy} \\ -2\boldsymbol{S}^w_{,xy} \end{bmatrix}^\top \boldsymbol{D} \begin{bmatrix} -\boldsymbol{S}^w_{,xx} \\ -\boldsymbol{S}^w_{,yy} \\ -2\boldsymbol{S}^w_{,xy} \end{bmatrix} dxdy\end{aligned} \tag{12}$$

The second integral of Eq. (11) becomes the geometric stiffness matrix of the finite element $\boldsymbol{K}_{G_{0e}}$, capturing the geometrically nonlinear effects of a pre-buckling membrane stresses $\boldsymbol{N}_0 = \{N_{0xx}, N_{0yy}, N_{0xy}\}^\top$

on the membrane stiffness. Noting that $\delta^2\boldsymbol{\kappa} = \mathbf{0}$ [51,52], the equation for $\boldsymbol{K}_{G_{0e}}$ becomes:

$$\boldsymbol{K}_{G_{0e}} = \iint_{xy} \begin{bmatrix} \boldsymbol{S}_{,x}^{w\top} N_{0xx} \boldsymbol{S}_{,x}^{w} \\ \boldsymbol{S}_{,y}^{w\top} N_{0yy} \boldsymbol{S}_{,y}^{w} \\ \boldsymbol{S}_{,y}^{w\top} N_{0xy} \boldsymbol{S}_{,x}^{w} + \boldsymbol{S}_{,x}^{w\top} N_{0xy} \boldsymbol{S}_{,y}^{w} \end{bmatrix} dxdy \tag{13}$$

The contributions all n_e finite element are added to build the global constitutive stiffness matrix $\boldsymbol{K}$ and geometric stiffness matrix $\boldsymbol{K}_{G_0}$ of the system:

$$\begin{aligned} \boldsymbol{K} &= \sum_{e=1}^{n_e} \boldsymbol{K}_e \\ \boldsymbol{K}_{G_0} &= \sum_{e=1}^{n_e} \boldsymbol{K}_{G_{0e}} \end{aligned} \tag{14}$$

The pre-buckling stress field of one BFSC finite element $N_{0xx}, N_{0yy}, N_{0xy}$ is calculated from the corresponding nodal displacements $\boldsymbol{u}_{0_e}$ as:

$$\boldsymbol{N}_0 = \begin{Bmatrix} N_{0xx} \\ N_{0yy} \\ N_{0xy} \end{Bmatrix} = \boldsymbol{A} \begin{bmatrix} \boldsymbol{S}_{,x}^{u} \\ \boldsymbol{S}_{,y}^{v} \\ \boldsymbol{S}_{,y}^{u} + \boldsymbol{S}_{,x}^{v} \end{bmatrix} \boldsymbol{u}_{0_e} \tag{15}$$

where $\boldsymbol{u}_{0_e}$ is directly extracted from the full pre-buckling displacement vector $\boldsymbol{u}_0$ that is obtained from a static analysis, derived from the equilibrium of Eq. (9):

$$\boldsymbol{u}_0 = \boldsymbol{K}^{-1} \boldsymbol{f}_0 \tag{16}$$

with $\boldsymbol{f}_0$ representing any general pre-buckling force. When applying the neutral equilibrium criterion of Eq. (11), one assumes that at the bifurcation point there is a value of internal membrane stresses $\boldsymbol{N}$ based on the known pre-buckling stress $\boldsymbol{N}_0$ described by $\boldsymbol{N} = \lambda \boldsymbol{N}_0$ that leads to the condition $\delta^2\phi = 0$. Therefore, the linear buckling problem consists of finding the value of λ that leads to:

$$\delta\boldsymbol{u}^{\top} \left(\boldsymbol{K} + \lambda \boldsymbol{K}_{G_0} \right) \delta\boldsymbol{u} = 0 \tag{17}$$

which holds true for any variation $\delta\boldsymbol{u}$, such that the required condition for the equality of Eq. (17) is the linear buckling equation given by:

$$\det \left(\boldsymbol{K} + \lambda \boldsymbol{K}_{G_0} \right) = 0 \tag{18}$$

Data availability

All models, optimisation algorithms and datasets generated and analysed during this study are publicly available under an MIT license [53].

References

[1] Izzi MI, Montemurro M, Catapano A, Pailhès J. A multi-scale two-level optimisation strategy integrating a global/local modelling approach for composite structures. Compos Struct 2020;237:111908. http://dx.doi.org/10.1016/j.compstruct.2020.111908.

[2] Picchi Scardaoni M, Izzi MI, Montemurro M, Panettieri E, Cipolla V, Binante V. Multi-scale deterministic optimisation of blended composite structures: case study of a box-wing. Thin-Walled Struct 2022;170:108521. http://dx.doi.org/10.1016/j.tws.2021.108521.

[3] Vannucci P, Verchery G. A special class of uncoupled and quasi-homogeneous laminates. Compos Sci Technol 2001;61(10):1465–73. http://dx.doi.org/10.1016/S0266-3538(01)00039-2.

[4] Vannucci P. Plane anisotropy by the polar method. Meccanica 2005;40(4):437–54. http://dx.doi.org/10.1007/s11012-005-2132-z.

[5] Montemurro M. An extension of the polar method to the First-order Shear Deformation Theory of laminates. Compos Struct 2015;127:328–39. http://dx.doi.org/10.1016/j.compstruct.2015.03.025.

[6] Montemurro M. The polar analysis of the Third-order Shear Deformation Theory of laminates. Compos Struct 2015;131:775–89. http://dx.doi.org/10.1016/j.compstruct.2015.06.016.

[7] Melo JDD, Bi J, Tsai SW. A novel invariant-based design approach to carbon fiber reinforced laminates. Compos Struct 2017;159:44–52. http://dx.doi.org/10.1016/J.COMPSTRUCT.2016.09.055.

[8] Tsai SW, Melo JDD. An invariant-based theory of composites. Compos Sci Technol 2014;100:237–43. http://dx.doi.org/10.1016/j.compscitech.2014.06.017.

[9] Tsai S. Double–double: New family of composite laminates. AIAA J 2021;59:4293–305. http://dx.doi.org/10.2514/1.J060659.

[10] Tsai SW, Arteiro A, Melo JD. A trace-based approach to design for manufacturing of composite laminates. J Reinf Plast Compos 2016;35(7):589–600. http://dx.doi.org/10.1177/0731684415624770.

[11] Tsai SW, Melo JDD, Sihn S, Arteiro A, Rainsberger R. Composite Laminates: Theory and practice of analysis, design and automated layup. Stanford Aeronautics & Astronautics; 2017, p. 136.

[12] Targino T, Cunha R, Medeiros A, Cardoso C, da Costa Ferreira EP, Melo JDD, Júnior RF. Damage resistance and damage tolerance of a double-double fiber-reinforced polymer composite laminate to impact. J Compos Mater 2024;58:2555–64. http://dx.doi.org/10.1177/00219983241274617.

[13] Riccio A, Garofano A, Caprio FD. Investigation on the crashworthiness of a composite fuselage barrel with double–double designed frames. Macromol Symp 2024;413. http://dx.doi.org/10.1002/masy.202300183.

[14] Nielsen MW, Butler R, Rhead AT. Minimum mass laminate design for uncertain in-plane loading. Compos Part A: Appl Sci Manuf 2018;115:348–59. http://dx.doi.org/10.1016/J.COMPOSITESA.2018.09.028.

[15] Shrivastava S, Sharma N, Tsai S, Mohite P. D and DD-drop layup optimization of aircraft wing panels under multi-load case design environment. Compos Struct 2020;248. http://dx.doi.org/10.1016/j.compstruct.2020.112518.

[16] Vermes B, Tsai S, Riccio A, Caprio FD, Roy S. Application of the Tsai's modulus and double-double concepts to the definition of a new affordable design approach for composite laminates. Compos Struct 2021;259. http://dx.doi.org/10.1016/j.compstruct.2020.113246.

[17] Vijayachandran A, Waas A. On the use of non traditional stacking to maximize critical buckling loads in flat composite panels. Compos Struct 2021;261. http://dx.doi.org/10.1016/j.compstruct.2020.113320.

[18] Xu Y, Gao Y, Wu C, Fang J, Sun G, Steven G, Li Q. On design of carbon fiber reinforced plastic (CFRP) laminated structure with different failure criteria. Int J Mech Sci 2021;196. http://dx.doi.org/10.1016/j.ijmecsci.2020.106251.

[19] Vermes B, Tsai S, Massard T, Springer G, Czigany T. Design of laminates by a novel "double–double" layup. Thin-Walled Struct 2021;165. http://dx.doi.org/10.1016/j.tws.2021.107954.

[20] Furtado C, Pereira L, Tavares R, Salgado M, Otero F, Catalanotti G, Arteiro A, Bessa M, Camanho P. A methodology to generate design allowables of composite laminates using machine learning. Int J Solids Struct 2021;233. http://dx.doi.org/10.1016/j.ijsolstr.2021.111095.

[21] York CB. Laminate stiffness tailoring for improved buckling performance. Thin-Walled Struct 2021;161:107482. http://dx.doi.org/10.1016/J.TWS.2021.107482.

[22] Zhang Z, Zhang Z, Caprio FD, Gu G. Machine learning for accelerating the design process of double-double composite structures. Compos Struct 2022;285. http://dx.doi.org/10.1016/j.compstruct.2022.115233.

[23] da Cunha RD, Targino T, Cardoso C, da Costa Ferreira EP, Júnior RF, Melo JDD. Low velocity impact response of non-traditional double-double laminates. J Compos Mater 2023;57:1807–17. http://dx.doi.org/10.1177/00219983231163513.

[24] Zhao K, Kennedy D, Miravete A, Tsai S, Featherston C, Liu X. Defining the design space for double–double laminates by considering homogenization criterion. AIAA J 2023;61:3190–203. http://dx.doi.org/10.2514/1.J062639.

[25] Wang Y, Wang D, Zhong Y, Rosen D, Li S, Tsai S. Topology optimization of Double-Double (DD) composite laminates considering stress control. Comput Methods Appl Mech Engrg 2023;414. http://dx.doi.org/10.1016/j.cma.2023.116191.

[26] Garofano A, Sellitto A, Acanfora V, Caprio FD, Riccio A. On the effectiveness of double-double design on crashworthiness of fuselage barrel. Aerosp Sci Technol 2023;140. http://dx.doi.org/10.1016/j.ast.2023.108479.

[27] Alves G, Vignoli L, Neto R. Damage onset in CFRP single lap joint for DD and QUAD laminates. J Mech Sci Technol 2024;38:157–62. http://dx.doi.org/10.1007/s12206-023-1213-z.

[28] Neto RMC, Vignoli L, Moreira C, Rohem N, Sampaio E. Increase of shear fracture energy of adhesive joints using double-double laminates. J Adhes 2024;100:1460–78. http://dx.doi.org/10.1080/00218464.2024.2318376.

[29] Kappel E. On the double-double laminate buckling optimum for the 18-panel 'horse-shoe' reference case. J Compos Sci 2024;8. http://dx.doi.org/10.3390/jcs8020077.

[30] Li Y, Qin H, Tan V, Jia L, Liu Y. A deep transfer learning approach to construct the allowable load space of notched composite laminates. Compos Sci Technol 2024;247. http://dx.doi.org/10.1016/j.compscitech.2024.110432.

[31] Zhao M, Zhao Y, Wang A, Chang Z, Zhang J, Wang Z. Investigation of the mode-I delamination behavior of Double-Double laminate carbon fiber reinforced composite. Compos Sci Technol 2024;248. http://dx.doi.org/10.1016/j.compscitech.2024.110463.

[32] Garofano A, Sellitto A, Caprio FD, Riccio A. On the use of double-double design philosophy in the redesign of composite fuselage barrel frame components. Polym Compos 2024;45:4250–65. http://dx.doi.org/10.1002/pc.28056.

[33] Riccio A, Caprio F, Tsai S, Russo A, Sellitto A. Optimization of composite aeronautical components by Re-designing with double-double laminates. Aerosp Sci Technol 2024;151. http://dx.doi.org/10.1016/j.ast.2024.109304.

[34] Zhao M, Wang S, Liu Z, Chang Z, Wang Z, Kang Y. A semi-analytical method for determining the mode-I delamination R-curve and fiber bridging traction-separation law of Double-double laminates. Thin-Walled Struct 2024;205. http://dx.doi.org/10.1016/j.tws.2024.112383.

[35] Zerbst D, Tönjes L, Dähne S, Werthen E, Kappel E, Hühne C. Equivalent plate formulation of Double–Double laminates for the gradient-based design optimization of composite structures. Compos Struct 2025;354. http://dx.doi.org/10.1016/j.compstruct.2024.118786.

[36] Fang P, Gao T, Huang Y, Song L, Liu H, Duysinx P, Zhang W. Uniform multiple laminates interpolation model and design method for double–double laminates based on multi-material topology optimization. Comput Methods Appl Mech Engrg 2025;433. http://dx.doi.org/10.1016/j.cma.2024.117492.

[37] Shabani P, Li L, Laliberte J. Low-velocity impact (LVI) and compression after impact (CAI) of Double-Double composite laminates. Compos Struct 2025;351. http://dx.doi.org/10.1016/j.compstruct.2024.118615.

[38] Vasconcelos T, Alves J, da Costa Ferreira EP, Júnior RF, Melo JDD. Static and fatigue behavior of double-double glass/epoxy laminates. J Compos Mater 2025;59:119–33. http://dx.doi.org/10.1177/00219983241261065.

[39] Lupu B, Loja M. Modeling and analysis of Double-Double composite structures integrating piezoelectric materials. Mech Adv Mater Struct 2025;32:15–33. http://dx.doi.org/10.1080/15376494.2024.2338910.

[40] Avila AF, Mapa L. QUAD and DOUBLE-DOUBLE laminates under cylindrical bending: A virtual characterization study. In: AIAA SCITECH 2025 forum. 2025, http://dx.doi.org/10.2514/6.2025-0574.

[41] Wang D, Su Z, Narayanaswamy S, Tsai SW. Buckling optimization of Double-Double (DD) laminates with gradual thickness tapering. Compos Struct 2025;351:118568. http://dx.doi.org/10.1016/j.compstruct.2024.118568.

[42] Kappel E. Buckling of simply-supported rectangular Double–Double laminates. Compos Part C: Open Access 2023;11. http://dx.doi.org/10.1016/j.jcomc.2023.100364.

[43] Blank J, Deb K. Pymoo: Multi-objective optimization in Python. IEEE Access 2020;8:89497–509.

[44] Riche RL, Haftka RT. Optimization of laminate stacking sequence for buckling load maximization by genetic algorithm. AIAA J 1993;31(5):951–6. http://dx.doi.org/10.2514/3.11710.

[45] Picchi Scardaoni M, Montemurro M. Convex or non-convex? On the nature of the feasible domain of laminates. Eur J Mech A Solids 2021;85:104112. http://dx.doi.org/10.1016/j.euromechsol.2020.104112.

[46] Gunduz M, Aslan M. DJAYA: A discrete Jaya algorithm for solving traveling salesman problem. Appl Soft Comput 2021;105:107275. http://dx.doi.org/10.1016/j.asoc.2021.107275.

[47] Barbero EJ, Reddy JN, Teply JL. General two-dimensional theory of laminated cylindrical shells. AIAA J 1990;28(3):544–53. http://dx.doi.org/10.2514/3.10426.

[48] Reddy JN. Mechanics of laminated composite plates and shells. 2nd ed.. CRC Press; 2003, http://dx.doi.org/10.1201/b12409.

[49] Donnell L. Stability of thin-walled tubes under torsion. Tech. Rep. 479, NACA Report No. 479, 1933, p. 22.

[50] Donnell LH. A new theory for the buckling of thin cylinders under axial compression and bending. Trans ASME 1934;56(11):795–806.

[51] Castro S, Jansen E. Displacement-based formulation of Koiter's method: Application to multi-modal post-buckling finite element analysis of plates. Thin-Walled Struct 2021;159:107217. http://dx.doi.org/10.1016/j.tws.2020.107217.

[52] Castro S, Mittelstedt C, Monteiro F, Arbelo M, Ziegmann G, Degenhardt R. Linear buckling predictions of unstiffened laminated composite cylinders and cones under various loading and boundary conditions using semi-analytical models. Compos Struct 2014;118:303–15. http://dx.doi.org/10.1016/j.compstruct.2014.07.037.

[53] Almeida Jr JHS, Balonek E, Castro SGP. Dataset for beyond double-double theory: n-directional stacking sequence optimisation in composite laminates. 2025, http://dx.doi.org/10.5281/zenodo.15864525.